EVALUATION OF THE EFFECTS OF ACTIVATION DEPENDENT REGULATION OF CD40L ON GERMINAL CENTER RESPONSE USING CD40LΔ5 MOUSE MODEL

By

BITHA NARAYANAN

A dissertation submitted to the

School of Graduate Studies

Rutgers, The State University of New Jersey

In partial fulfillment of the requirements

For the degree of

Doctor of Philosophy

Graduate Program in Microbiology and Molecular Genetics

written under the direction of

Lori R. Covey

and approved by

_____

_____

_____

_____

New Brunswick, New Jersey

January 2020

ABSTRACT OF THE DISSERTATION

ACTIVATION-DEPENDENT POSTTRANSCRIPTIONAL REGULATION OF CD40L IS REQUIRED FOR AN OPTIMAL GERMINAL CENTER (GC) RESPONSE.

by BITHA NARAYANAN

Dissertation Director

Dr. Lori R. Covey

The interaction between cognate T and B cells decides the progression of an immune response to a pathogen or self-antigen. Of the multiple signals that synchronize to fine-tune this union, the binding of CD40 on the surface of B cells to CD40L expressed on CD4 T cells is of paramount importance. Ligation of CD40 on antigen-experienced B cells is associated with the initiation and development of germinal centers (GCs) resulting in the subsequent generation of high affinity antibodies and B cell memory. Post-transcriptional regulation of CD40L has been implicated in regulating the activation dependent expression of this protein. Our lab has previously shown a polypyrimidine tract binding protein complex binds to the 3' UTR of the CD40L mRNA

and that the deletion of a PTBP1 binding stability element in the same results in a significant decrease in the half-life of the CD40L transcript and subsequently the surface expression at later stages of activation *in vitro*. To understand the biological basis for activation-induced posttranscriptional regulation of CD40L, a mouse was engineered with a deletion of two segments in the PTBP1 stability element that provide stability to the transcript and termed CD40LΔ5 (data not shown, work done by K. Voskoboynik and J. La Porta). Notably, splenic CD4 cells from the CD40LΔ5 mouse showed decreased CD40L expression at later stages following *ex vivo* activation.

It has been well established that CD40L knock-out mice are unable to surmount an adequate immune response when subject to antigen challenge. The question we asked was whether the activation-induced pathway of CD40L mRNA stability was required to achieve an optimal immune response. It has been shown that GC B cells constantly shuttle between the T follicular (T_{fh}) rich, light zone (LZ) and the dark zone (DZ) where they undergo somatic hypermutation. B cells rely on interactions with the T_{fh} cells to provide direction as to how to evolve to optimize the immune response. We hypothesized that this interaction would be disrupted in CD40LΔ5 mice and subsequently result in the T_{fh} cells being unable to provide durable support to the B cells to develop into functioning antibody factories.

To test our hypothesis, we assessed the immune response in CD40LΔ5 and wild type mice in response to a T dependent antigen, NP-KLH. We observed significantly reduced levels of antigen-specific antibodies in the mutant mice when compared to the wild type by ELISA. On evaluating whether this decreased antibody generation was subsequent to a reduced number of plasma cells (by ELISPOT), we found that there was

indeed a decrease in the number of NP-KLH specific clones of plasma cells in the CD40LΔ5 mice. The splenic sections from WT and mutant mice revealed that the mutant mice were able to produce GCs in contrast to the CD40L knock out mice, but these GCs were much less organized with scattered GL7 (marker of GC B cells) positive cells when compared to the wildtype where distinct GL7 positive cores were surrounded by IgD positive rings. This data suggested that the CD40LΔ5 is allowing for seeding and initiation of GCs, but at subsequent stages, deregulated CD40L results in less effective development of the immune response.

Based on phenotypic and genotypic evaluation we conclude that the CD40LΔ5 mice have reduced number of organized GCs and in turn lower levels of antibody secreting plasma cells and consequently lower titers of antibodies from isotypes IgG1, IgG2b, IgG2c, and IgM against NP. We also found decreased affinity maturation in the CD40LΔ5 mice, but the SHM rate was similar to that of the wild type. In addition, the alteration in CD40L mRNA stability alters the development of the memory B cell and long-term plasma cell populations. When we looked at differentially expressed genes by RNAseq, several genes associated with proliferation were down regulated in the CD40LΔ5 mice. On the contrary, genes linked to apoptosis were upregulated in the CD40LΔ5. We were able to confirm this pattern by flow cytometry on GC B cells. The sum total of our data strongly supports a major role for the posttranscriptional pathway of CD40L mRNA stabilization for regulating expression and ensuring the timely availability of CD40L on T_{fh} cells to signal activated B cells to produce a robust humoral response.

Acknowledgements

I would like thank Dr. Covey for her relentless support and mentoring through my very difficult time schedule and constraints. Without her guidance and understanding I would never have been able to achieve my goal. She taught me how to think outside the box and challenge myself when I came across hurdles. I will value the lessons that I learned from her throughout my life.

I would like to thank Dr. Xie for all her recommendations and suggestions for how to address each issue we had and her extensive understanding of our project and its intricacies. I would like to thank Dr. Kiledjian for all his advice and suggestions that helped us fine tune our experiments. I would like to thank Dr. Sant' Angelo for infusing his enthusiasm into our data and inspiring us to shoot for the high bar.

I would like to thank Diego and Usha for being wonderful lab mates and supporting me through my unwieldy schedule, making me laugh and being good friends. I would like to thank Sue (Schwander's lab) and Beth and Valentina (Margolis lab) for all their support.

I would like to acknowledge the extensive administrative support that exists for students at Rutgers. I would specifically like to thank Diane Murano our administrative beacon for all her support and help during every step of the way during my post-graduate school. I wouldn't have been able to finish my doctorate without her timely support.

I would like to dedicate my work to past and present mentors at Pfizer, Bracco and Antyra for all their support and the training they provided me. Without the encouragement and support from Dr. Dangshe Ma, I wouldn't have embarked on this

journey. I would also like to thank Pfizer for funding my education, without which I would not have been able to achieve my aspirations.

Last but not least I would like to thank my parents, my children and my husband for providing unconditional support throughout my journey and hope that someday I will be able to make them proud.

Table of Contents

List of Tables

List of Figures:

Introduction

The cyclical progression of cell proliferation, differentiation and cell death is intricately regulated by a multitude of events from the initiation of transcription of the germline DNA sequences to translation [1-9]. The mammalian immune system is fine tuned to regulate the levels of activation associated proteins through multiple signals like cytokines, nutrients, hormones and temperature as well as through transcriptional and posttranscriptional modifications. The regulation of protein expression through posttranscriptional mRNA stability has received more attention in the past two decades. The mRNA untranslated regions (UTRs) have been shown to play an important role in the regulation of mRNA stability, export to the cytoplasm, sub-cellular localization and translation, ultimately regulating the total protein synthesis [10, 11] [12]. mRNAs with higher rate of turnover are more sensitive to transcription levels than those that have a longer half live [13]. Thus, mRNA of some molecules which are essential for activation in the immune response have shorter half-lives and additionally bind proteins regulated by activation that can protect the mRNA from constitutively active endonucleases depending on the needs of the system [14-16]. Expression of proteins essential for initiation and resolution of inflammation is regulated by RNA binding proteins (RBPs) that either affect the stability of their transcripts or the subsequent translation [3]. Expression levels of these proteins are consequently modulated in response to activation, sometimes by the RNA they protect [17, 18]. CD40L is activation induced receptor which is expressed on helper T cells and is delicately regulated by the binding of a stabilizing protein complex, (PTBP1 complex) to the 3'UTR of its transcript.

Role of RNA binding proteins in activation dependent regulation of mRNA

After transcription, the nascent transcript is subject to multiple posttranscriptional modifications and potential degradation by nucleases in the cytoplasm. Its fidelity is dependent on the binding of sequence-specific RBPs [18-20]. Subsequently, depending on the levels and modification of RBPs, such as phosphorylation, mRNA levels are regulated, and down-stream protein levels are controlled [17, 18].

CD40L (ligand for CD40) expressed on T cells is an essential immune component that is regulated at multiple levels through transcriptional, post-transcriptional and translational modifications. When immune activation progresses, the extracellular signals drive modifications of RBPs leading to modulation of transcriptional and posttranscriptional changes in RNA for activation induced proteins like CD40L [21-24].

The Polypyrimidine tract-binding protein 1 or PTBP1, binds to the polypyrimidine tracts in the introns of pre-mRNA, promotes binding of U2 snRNP to the pre-mRNA and functions in splicing through the protein degradation ubiquitin-proteasome pathway [25-30]. When the PTBP1 binding site is located upstream of an exon, or within it, PTBP1 usually acts as a splicing repressor [31], conversely, if it binds downstream of the exon it enhances splicing [32]. In addition to its site- specific splicing function, PTBP1 also acts as in RNA transport between the nucleus and cytoplasm where it acts at critical steps of RNA biogenesis, stabilizing the mRNA from decay [29, 33]. PTBP1 needs to be phosphorylated by the 3′,5′-cAMP-dependent protein kinase, so that it can be exported into the cytosol [34]. It is known to form complexes with companion proteins, like nucleolin, bind to the mRNA and protect it from degradation [29, 35, 36]. *In vitro* studies conducted in our lab showed that posttranscriptional regulation of CD40L

was closely associated with an activation-mediated binding of PTBP1 to the CD40L mRNA and subsequent regulation of mRNA decay at late times of activation. We also demonstrated that PTBP1 effectively reduced degradation of the CD40L mRNA at later stages of activation [36, 37]. Here we strive to understand the *in vivo* implications of this pathway, which micro-regulates the CD40L expression in an activation dependent manner, in a mouse model with a deletion in the CD40L stability element.

T-dependent immune cascade

The humoral response to an antigen challenge or an infection is a complex cascade of intricately regulated events. When a T-dependent antigen enters the immune system, the sentinels of the immune system, the macrophages and dendritic cells, phagocytose the protein and prime resting T cells to peptides presented on MHC from the internalized antigens. This triggers multiple costimulatory signals and the activated T cells subsequently respond to the cognate peptide presented by B cells on MHC class II, providing cell surface and secretory signals to B cells [38, 39]. B cells need an ancillary signal from a cognate CD4 T helper cell to function effectively [40]. The interface between CD40 on B cells and CD40L on the CD4 T cells is a critical component in the interaction between the two cell types [41]. The CD40L knock out mice has a severely compromised T dependent immune response [42].

A secondary high affinity humoral response follows the initial low affinity predecessors after several rounds of random mutation and affinity maturation. This phenomenon happens in germinal centers (GCs) formed within the follicles of secondary lymphoid organs following the introduction of an infecting pathogen or other immunogen [43, 44] [45-49]. The CD4 helper T cells that migrate into the GCs, T_{fh} cells, express high

levels of CXCR5 and PD-1 on their surface and the transcription factor Bcl6 and upregulate CD40L upon activation [50]. Although GC development is dependent to various degrees on the species, the presence of T_{fh} cells, the immunogen, and the secondary lymphoid organ where the response occurs [51-55], all GCs are seeded by antigen activated B cells that initiate a humoral immune response. The activated B cells interact with the cognate T cells expressing CD40L in the T cell zone border. The CD40L expression on the T cells is essential for this initial interaction between the B and T cells. The activated B cells then move into the center of B cell follicles and proliferate forming GCs [51, 55]. The GC B cells undergo a series of somatic hypermutation (SHM) of their immunoglobulin genes that is dependent on the activation-induced cytidine deaminase or AID enzyme, in specific regions of the GC called the dark zone (DZ) [56] [57]. The B cells with mutations that increase their ability to bind specific antigen, are then selected to interact with a limiting number of T_{fh} cells, in regions of the GC called the light zone (LZ). The B cell clones that lack the specificity or are unable to interact with the $T_{fh,}$ undergo apoptosis in the LZ [49, 58]. The effectiveness of the interaction of GC B cells with the T_{fh} is dependent on the level of expression of CD40 on B cells and CD40L on the T_{fh}.

The B cell clones with higher affinity are repeatedly selected by interactions with the T_{fh} cells in the LZ. The availability of surface CD40L is essential for the T_{fh}-GC-B cell contact at each recurrence and hypothetically disruption of this signal would have drastic downstream impact. After the high affinity clones are selected (affinity-maturation) GC B cells can either return to the GC DZ for further modifications or differentiate into memory B cells or long-lived plasma cells. The strength and duration

of the T_{fh}-GC-B interaction regulates the fate of the B cells with more robust signals directing differentiation into plasma cells and GC B cells, while attenuated signals support memory B cell differentiation [59]. CD40L signal is essential for effective T_{fh}-GC-B union and the extent of this signal affects the differentiation pathway for GC B cells. High affinity B cells are able to present antigen-derived peptides on their MHC class II and can induce upregulation of CD40L in the T_{fh} [41].

Light zone/Dark zone Dynamics

The GC LZ is occupied mainly by FDCs and T_{fh} cells whereas the DZ has activated CD19+B220+ B cells that are tightly packed and actively proliferating. The DZ GC B cells or centroblasts express high levels of chemokine receptor CXCR4 polarizing them towards CXCL12, its ligand, secreted by CXCL12-expressing reticular cells (CRCs) in the DZ [60, 61]. On the contrary, CXCL13/CXCR5 chemokine/receptor pair is needed for GC B cells to accumulate normally in the LZ and CXCL13 is secreted by FDCs in the LZ [60, 62]. Upregulation and downregulation of surface CXCR4 expression seems to be the mechanism that encourages the movement of GC B cells between the two zones [60]. As GC B cells cycle between the LZ and the DZ, the clones that are able to get sufficient T_{fh} help, proliferate and are further selected for high affinity mutation. Effective T_{fh} help is reliant on sufficient CD40L expression. During the progression of GC development, B cell interclonal selection advances to competition between variants of a single clone generated by SHM [63]. LZ to DZ migration is constrained by availability of GC-resident T_{fh} and CD40/CD40L interaction [64]. If T_{fh} cells are not limiting, but CD40L is attenuated, there would be reduced T_{fh} help, and the GC B cells will have reduced ability to re-present antigen [65].

Somatic Hypermutation and Affinity maturation

Activation-induced cytidine deaminase (AID), needed for somatic hypermutation and class switch recombination, is primarily expressed in the DZ in GCs [56, 66, 67]. In response to the antigen hapten 4-hydroxy-3-nitrophenylacetyl (NP), selection for a mutation of Trp33 to Leu in V_h186.2 occurs in the GC within two weeks and provides 10-fold higher affinity, but 6 weeks later an additional mutation results in Trp33 to Gly99 which has an even higher affinity [68]. GC DZs have been long thought of as the primary sites for SHM. CD40L knock out mice do not develop GCs. So, it would be plausible to postulate that SHM would be dependent on CD40L expression. But, a recent report from di Niro et.al., has shown that SHM in mice can happen effectively in microdissection of extrafollicular regions, in the context of infectious agent driven immune response, and this in turn can result in affinity maturation. Despite initial promiscuity in clonal selection, the extrafollicular response yielded high affinity antibodies against Salmonella infection [69]. This contradicts the initial belief that GCs are essential for SHM. However, the CD40/ CD40L interaction is still indispensable for the initial interaction between the T and B cells.

Class-switch Recombination

Class-switch recombination (CSR) is an intrachromosomal DNA rearrangement of the immunoglobulin (Ig) heavy-chain locus. IgM-IgD mature B cells undergo class-switch recombination (CSR), which involves DNA rearrangement of the immunoglobulin (Ig) heavy-chain locus. This generates antibodies of the IgA, IgG, or IgE classes with different effector functions while retaining the specificity for the immunogen [70]. GCs have been long believed to be the primary site for CSR [71, 72]. However, extrafollicular

CSR has also been detected early during the primary immune response (day 2) [53, 73, 74]. Roco et.al. demonstrated that CSR is initiated within the few days of immunogen exposure and before development of GCs and terminates soon after B cells become GC cells [75]. Despite this, in the absence of GCs, CSR is still impacted significantly. In Hyper-IgM syndrome with CD40L deficiency, marked decrease in isotype switched IgG and IgA with normal or elevated IgM levels is observed [76].

T cell help and humoral immune response

Over the years considerable effort has gone into understanding the contribution of multiple elements that influence the GC development. The availability of T cell help is considered the most critical factor for successful GC development. During clonal selection of B cells, if CD40/CD40L interaction via T_{fh} is not limiting, the discrimination between cells of different affinity for the foreign antigen is based exclusively on the strength of BCR signaling [50, 77-79]. If ,on the other hand, there is competition for T_{fh} help, B cells that have captured, processed, and presented more antigen as MHC-peptide complexes receive T cell help at the expense of cells that have captured fewer antigens [50, 77]. Reduced CD40L creates a scenario where the GC B cells compete for the limiting resource or T_{fh} interaction and only the higher affinity B cells would plausibly succeed and survive.

Role of CD40L in the GC reaction

Costimulatory molecules CD40L, CD28 and ICOS as well as cytokines IL-4 and IL-21 are critical for the T helper response during GC development and function [80, 81] [82-84]. CD40L has been extensively studied for its role in the formation and survival of GCs, and the CD40L knock out mice do not form functional GC [85-87]. But the in vivo

kinetics of the signal and its impact through the progression of the immune response is much less understood [41]. Blocking the CD40/CD40L interaction at early stages of the immune response using an anti-CD40L antibody decreased serum titers by 90%, and although anti-CD40L treatment can abrogate an already established GC reaction, once the B cells are committed to a differentiation pathway CD40L is not needed for their differentiation and survival. [88]. This indicates that the CD40L expression dynamics are important for the effective functioning of GCs. The kinetics of CD40L expression is regulated in the GC by feed forward loops. For example, CD40L upregulates ICOSL on GC B cells, followed by a feed forward induction of additional CD40L expression on T_{fh} cells. This empowers high-affinity B cells to recurrently obtain more T cell help than the lower affinity clones [89].

Long lived plasma cells and memory B cells

Bone marrow (BM) long lived plasma cells (LLPCs) are derived from GCs [90, 91] [92, 93], but can also form in GC deficient $Bcl6^{-/-}$ animals [94] and in response to T-independent immunogens [95]. All memory B cells (MBCs) have not undergone class switching or SHM [96] [97] [98] Isotype-switched late stage MBCs are believed to originate in the GC while early non-switched MBC phenotypes are GC independent [53, 99, 100] [101]. Differentiation of GC B cells into MBCs and LLPCs has been extensively studied [46] [102] [49] [103].

CD40-mediated signaling with cytokines could have an impact on the MBC and LLPC decision [46, 102]. Blocking antibodies directed against CD40L or ICOSL results in a decrease of LLPCs and deletions in CR1 and CR2 [43], interleukin 21 receptor (IL-21R) [104, 105], PD-1, PD-L1, and PD-L2 [106] and CD80 [97] allow GC initiation but

prevent effective GC maturation or progression. If GC maturation is disrupted, it results in reduced LLPCs, but not MBCs [90].

The CD40LΔ5 model has a deletion in the 3'UTR of the CD40L transcript, which prevents binding of the PTBP1 complex to the stability element and makes the mRNA prone to faster degradation. This model does not have any mutations in the CD40L translated regions and does not eliminate CD40L expression completely. The PTBP1 complex binding to the stability element is contingent on activation mediated modifications to the PTBP1. The concept behind out model is that we still maintain normal levels CD40L in the naïve CD40LΔ5 mice. However, when exposed to an immunogen, the activation triggers the binding of the PTBP1 complex, stabilizing the mRNA of the WT mice. Conversely, the CD40LΔ5 transcripts are more susceptible to decay and subsequently have less CD40L surface expression.

We evaluated whether the decreased CD40L signaling in this model be sufficient to impact the GC formation and development. So as to address this question we evaluated the distribution of T and B cell subsets and studied the structure of the GCs. We observed a marked decrease in GC B cells, MBCs and plasma B cells but no difference in the T_{fh} cells in the CD40LΔ5 mice. The structure and distribution of the GCs also showed disruption in our model. We also addressed the question whether the activation induced mRNA stability pathway was critical for antibody production, class switching and somatic hypermutation. We estimated antibody titers from WT and CD40LΔ5 mice, compared the IgM levels and the isotype switched classes IgG1, IgG2b and IgG2c in the two genotypes. Decreases in all isotype switched antibody classes was observed in the CD40LΔ5 mice but very less impact was observed in the IgM isotype. We also detected

a significant reduction in the degree of affinity maturation and high affinity mutations in the CD40LΔ5 mice. We studied the gene expression profile by RNAseq and determined that several proliferation-associated genes were downregulated in the CD40LΔ5 mice. Here we strive to understand the consequences of activation dependent post-transcriptional regulation of CD40L mRNA, on the development of a humoral response.

Chapter I : Genotypic and Phenotypic Evaluation of CD40LΔ5 prior to antigen challenge

The cognate interactions between T and B cells mediate a series of events which consequently result in the generation of antibodies capable of specifically neutralizing antigens and pathogenic agents. The contact dependent interaction between the CD40L on the T cells and the CD40 on the B cell is essential for the development of high affinity antibodies capable of initiating an effective and specific immune response.

Previous data from our lab has shown that *in vitro* optimal expression of CD40L at late times of activation is dependent on a stability element located in the 3' untranslated region (UTR) of the CD40L transcript that is bound by an RNA complex (Complex I) containing polypyrimidine tract-binding protein (PTBP1) [37]. A deletion in the stabilizing region of the PTBP1 stability element in the CD40L mRNA consequently makes it susceptible to faster decay, When the stability element was disrupted *in vitro* during activation with αCD3/αCD28, CD4 cells show decreased mRNA stability and subsequently lower CD40L expression at later stages of activation.

Our primary question was whether the mRNA stability pathway is active *in vivo*. The CD40LΔ5 mouse model has a deletion in the stabilizing region of the PTB stability element in the 3'UTR of the CD40L mRNA. The CD40L translated protein is unmutated. To understand whether this deletion reduced CD40L expression available for B cell interaction *in vivo*, we provided *ex vivo* activation and measured surface CD40L. We found this was indeed the case and the next question we addressed was whether this decrease in surface CD40L can be correlated to decreased mRNA stability of the

transcript in CD4 cells from CD40LΔ5 mouse. Once we established that the pathway was indeed functional in this model, we evaluated whether the decrease in CD40L affects the distribution of the pre-immunization B and T cell subsets. No significant differences in the pre-immunization immune cell repertoire was observed. Based on these findings we concluded that the CD40LΔ5 mouse model is an effective tool to study the effect of the activation dependent mRNA stability pathway for CD40L.

Introduction:

CD40L is an activation induced surface receptor on CD4 T cells that is regulated during transcription, post transcriptionally and during translation by multiple mechanisms [37, 107-109]. Our lab focused on the post-transcriptional regulation of the CD40L transcript via binding of the PTBP1 complex to the 3' UTR of the mRNA. *In vitro* and *ex vivo* studies of CD4 T cell activation conducted at our lab, have shown that CD40L surface expression increases at later time points of activation [37, 110]. However, when we studied the mRNA at later stages of activation, there was a surprising decrease in the levels of CD40L mRNA. We established that the reason for this discrepancy was that at later stages of activation there was the increased stability of the CD40L mRNA due to the binding of the mRNA stabilizing PTBP1 complex and even with lower levels of mRNA, surface expression of CD40L is higher [37, 110]. The mouse CD40L mRNA was also shown to become stabilized in *in vivo* primed T cells following secondary exposure to KLH [110]. Based on this data we generated a mouse model, CD40LΔ5 that carries a deletion in a part of the stability element that stabilizes the binding of the PTBP1 complex and protects the CD40L mRNA.

Our question was whether destabilization of the PTBP1 complex binding to CD40L mRNA would indeed impact the surface expression and RNA levels of CD40L *in vivo*. We found the naïve CD40LΔ5 mice expressed lower levels of surface CD40L than the WT mice and this differential was apparent at relatively later stage of *ex vivo* activation (24 h) with αCD3/αCD28. We also discovered that the rate of degradation of CD40L transcript was accelerated in the CD40LΔ5 mice when compared to the WT, indicating that the PTBP1 mediated pathway was indeed affecting the CD40L expression in this model.

The CD40L knock out mice has been extensively studied over the past few decades [42, 85, 86]. Renshaw et.al. showed that the CD40L deficient mice had normal distribution of B and T cell subpopulations but had severely decreased basal serum levels [86]. It has also been shown that constitutive CD40L expression by naive CD4 T cells impacts the distribution of the B cell subsets and could in turn affect other cell types such as T regulatory cells (T_{fr}) [111]. The question pertinent to our model was whether the activation dependent mRNA pathway could affect pre-immunization levels of CD40L in a way that the distribution of naïve T and B cell subsets would be affected. To address this query, we evaluated the immune repertoire from naïve CD40LΔ5 and WT thymii, spleens and lymph nodes.

Material and Methods:

Mice

A region of the CD40L 3'UTR corresponding to the PTBP1-complex binding sites B and C (Δ5) (nt 900 -1086) was deleted by site-directed mutagenesis (data unpublished, K. Voskoboynik and J. La Porta) . Two loxp sites, located on either side of the Neo_r, were used for Cre recombination to remove the Neo_r cassette. Heterozygous C57BL/6 transgenic female mice carrying the Δ5 mutation were bred with a Cre deletor male (kind gift from Dr. Xie) to remove the Neo_r gene then cross bred over 3 generations to ensure the removal of the Cre gene.

Genotypic evaluation prior to immune challenge:

Validation of germline transmission was carried out by genomic PCR analysis of tail DNA. Long-amp PCR using CD40L genotyping primers (Table I-1) binding to either side of the stability element was used to genotype the mice into WT, heterozygous and homozygous mutant. The Cre fragment was detected using forward and reverse Cre primers (kind gift from Dr. Xie) and the Cre deletion was confirmed after 3 generations.

Cell isolation from tissues

Spleens, thymii and lymph nodes were collected from 6-10-week-old mice and subject to gentle mechanical dissociation between glass slides, then filtered using a 40-µm Falcon cell strainer and suspended in Hanks Buffered Saline solution (HBSS). For the spleens, red blood cells (RBCs) were lysed using 1X Ammonium-Chloride-Potassium (ACK). Following RBC lysis for 35 seconds using 1X ACK lysis buffer, the cells were washed

3X with HBSS containing 5% FBS and resuspended in RPMI with 10% FBS and counted.

Determination of mRNA stability

Splenic CD4 cells (5×10^6) were isolated by negative selection using the Mojo Sort Kit and activated for 6-24 h (based on identified time-points from preliminary experiments) in the presence of solid phase CD3 (10 µg/mL) and soluble CD28 (2µg/mL) antibodies. These cells were incubated in the presence of the RNA synthesis inhibitor DRB at a concentration of 50 µg/mL and 1 X 10^6 cells collected every 30 for 1.5 h. RNA was purified from the cells lysed with Trizol, using chloroform and ethanol precipitation and reverse transcribed using oligodT primers and Superscript RTII. For qPCR, β-2microglobulin was used as the endogenous control (Table I-1).

Flow Cytometric immunophenotyping:

For flow analysis, 1×10^6 splenocytes were suspended in PBS with 1% BSA and 2% rat serum with 1µg/mL of 2.4G2 (anti-FcγR) to block FcR binding. After 10 of incubation on ice, the appropriate primary antibodies were added to the cells at 1-10 µg/mL depending on the manufacturer's recommendation and incubated for half an hour on ice. The cells were washed twice with PBS containing 1% BSA, and secondary antibodies were added where necessary for another 30 on ice. The cells were washed twice in PBS and resuspended in 1% paraformaldehyde in PBS. Flow cytometric analysis was performed on a FACS Calibur or Fortessa cytometer.

Results:

Genotypic evaluation of the CD40LΔ5 model

The first task we faced was to validate the genotypic purity of the CD40LΔ5 model. Validation of germline transmission was carried out by genomic PCR analysis of tail DNA. Long-amp PCR using primers targeting either side of the Δ5 deletion was used to genotype the mice into WT, heterozygous and homozygous mutant . PCR results using Δ5 Forward and Δ5 reverse fragments (as described in the schematics, **Figure I-1**a) show the homozygous CD40LΔ5 mice with a single lower band running at 513 bp while the wild type band runs at around 691bp and the heterozygous mice carry both the aforementioned bands (**Figure I-1**b). The Neo_r gene was deleted by crossing the CD40LΔ5 with a Cre deletor mouse. We confirmed the deletion of the Neo_r and then the Cre-fragment was deleted from the mating pairs by repeated breeding. The Cre PCR would show bands at around 500 bp is indicating the presence of the remnant Cre fragment in 50% of the progeny if one of the parents carries the Cre fragment. No bands were observed with any of the breeding pairs and progeny indicating complete removal of the Cre fragment. The positive control lane 4 shows the position of the band if Cre is present. (**Figure I-1**c). Thus, we confirmed that the CD40LΔ5 mice we used for future breeding and experiments did not carry the Neo_r gene or the Cre fragment.

a

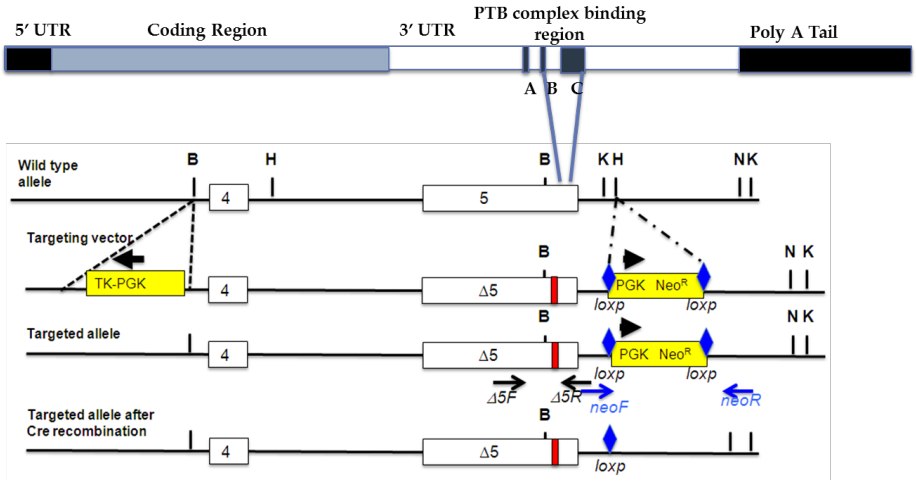

b 1Kb Y/- Y/+ Y/- +/- +/-

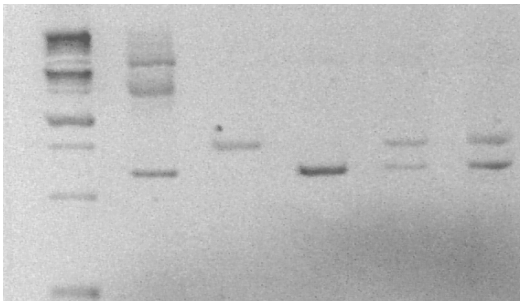

c 1Kb Y/- Y/+ Y/- Cre+Ctrl

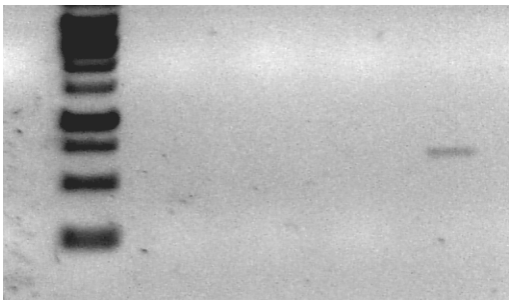

Figure I-1 Evaluation of CD40LΔ5 deletion by tail genomic DNA by PCR .
(a) PTB containing complex binding sites B and C (Δ5) in the 3'UTR sequences between 900 -1086, were deleted by site-directed mutagenesis. Two loxp sites, located on either side of the Neor, were used for Cre recombination to remove the Neor cassette. (b) Representative genotyping of individual mice was carried out using CD40L Δ5 forward and Δ5 reverse fragments (directed to either side of the Δ5 deletion) and generates a 691 bp fragment in the WT and a 513 bp fragment in the CD40LΔ5 mice. The heterozygous females have two bands one at 691 and the other at 513. The Cre PCR was run with Cre forward and reverse primers indicate the presence or absence of the Cre-fragment (c) Representative gel picture shows n=3 mice in lanes 1-3. Lane 4 shows positive control for Cre carrying mice.

Reduced CD40L expression observed in the stability element deleted mouse

Previous studies done in our lab show that the CD40LΔ5 deletion leads to decreased mRNA stability and consequently reduced CD40L expression after *in vitro* activation. To evaluate whether findings translate *in vivo* to CD4 T cells lacking the stability region, we collected splenocytes from wild type and CD40LΔ5 mice, isolated CD4+ T cells by negative selection, and activated them *in vitro* with plate-bound αCD3 with soluble αCD28 mAb for different lengths of time (0 h, 6 h, 12 h, 24 h and 48 h). Following activation, the CD40Lsurface expression was studied by flow cytometry. The CD40L expression in the CD40LΔ5 splenic CD4 T cells showed a modest decrease over the time course of activation when compared to the wild type mice and the difference was significant at the 12 h and 24 h time points (**Figure I-2**).

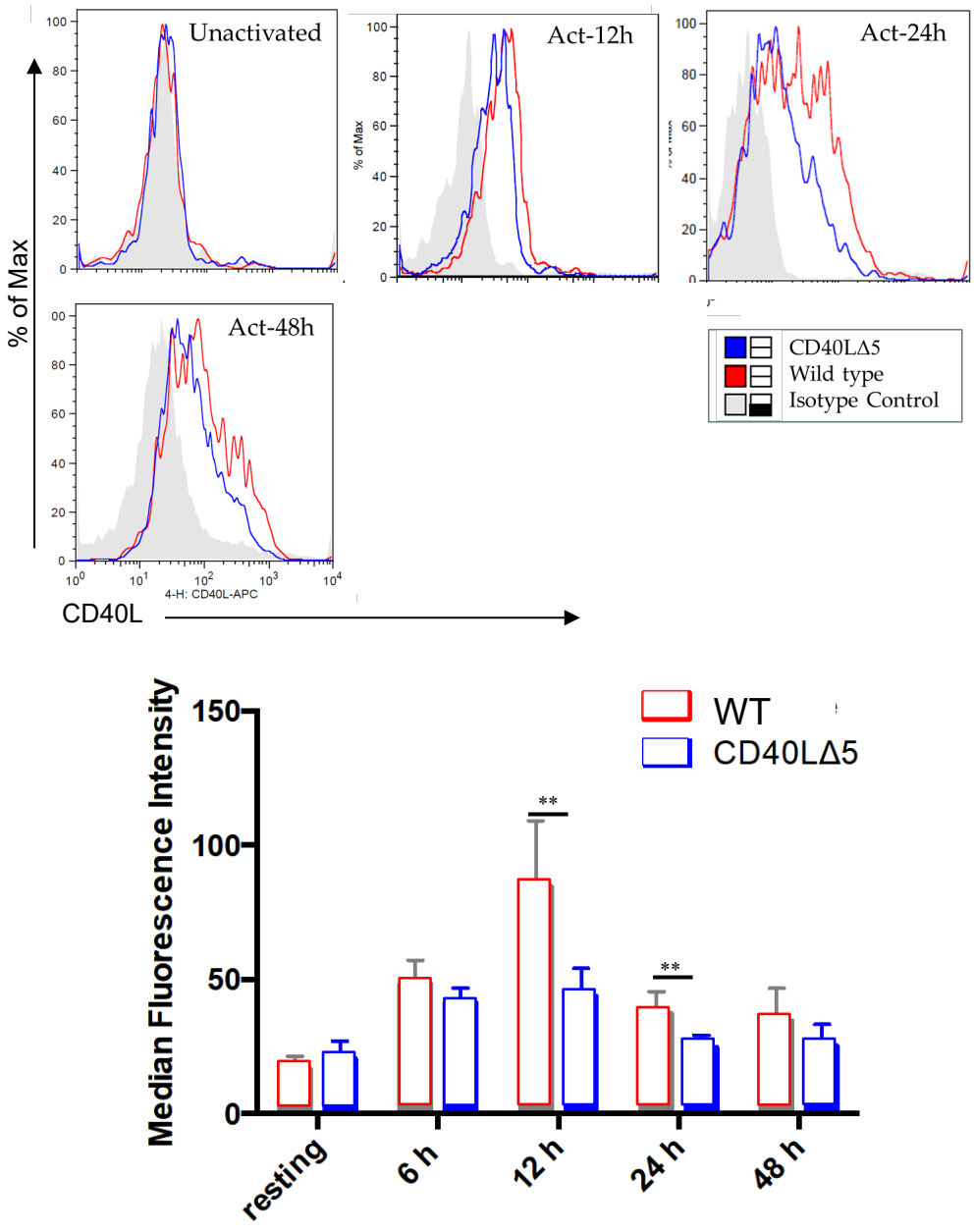

Figure I-2 Lowered CD40L surface expression in CD40LΔ5 splenic CD4 T cells. Splenic CD4+ T cells isolated by negative selection were activated *in vitro* with plate-bound anti-CD3 with soluble anti-CD28 mAb for different lengths of time (0 h, 6 h, 12 h, 24 h and 48h) CD40L expression in the CD40LΔ5 and wild type were compared by flow cytometry using a biotinylated αCD40L antibody followed by streptavidin APC secondary. (a) Representative plot from 3 different experiments and 6 mice shown. (b) Quantitation of mean fluorescence intensity of CD40L at 0 h, 6 h, 12 h, 24 h and 48h. Data represented as mean+/-SEM. Significance was assessed by student's unpaired t-test where *$p < 0.05$; and **$p < 0.005$ was considered significant.

In vitro, we have shown that the impact of the deletion has a direct effect on the stability of CD40L mRNA. To evaluate the effect of the pathway *in vivo*, we measured the rate of mRNA decay in the CD4 T cells isolated from WT and CD40LΔ5 mice in the presence of DRB. At the end of the 24-hour activation period, DRB was added to the activated CD4+ T cell cultures and samples were collected at time points between 0-90 mins. The decay of CD40L mRNA from CD40LΔ5 mice was compared to that of wild type mice. We see a 30% increase in the rate of CD40L mRNA decay in the CD40LΔ5 when compared to the wild type CD4 cells. (**Figure I-3).**

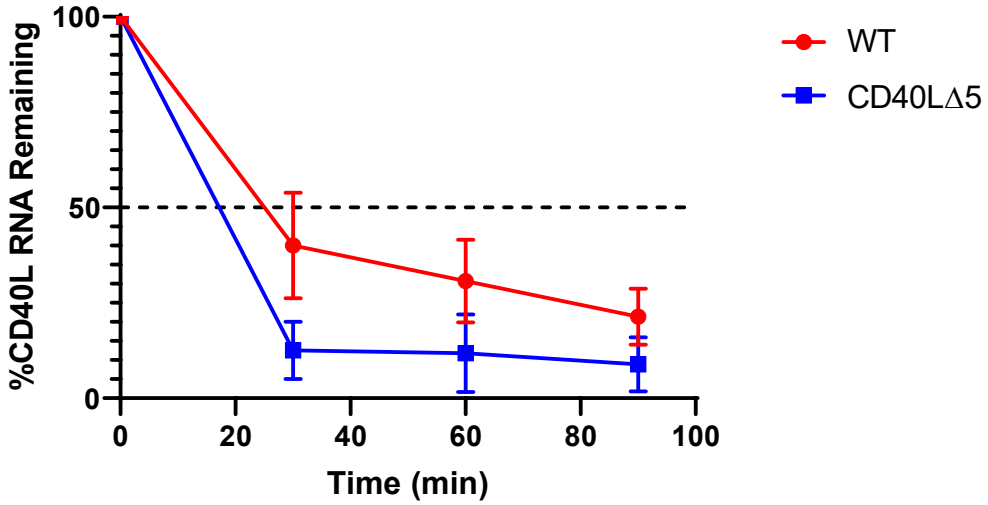

Figure I-3 The CD40LΔ5 deletion has a significant impact on the rate of mRNA decay, relative to the wild type, in the mutant CD4 T cells.
Isolated wild type and CD40LΔ5 splenic CD4 T cells were activated *ex vivo* with αCD3/αCD28 for 24 h. The activated cells were incubated in the presence of 50 μM of DRB for 0, 30, 60 and 90 min, then RNA was extracted. qPCR performed. Consolidated data from 3 independent experiments show the remaining CD40L mRNA from wild type (red) and CD40LΔ5 (blue). Data represents mean and SEM of 3 independent experiments.

Activation is not affected in the CD40LΔ5 model

CD69, an early inducible marker for activation, expressed on CD4 T cells, was used to evaluate whether the decrease in surface CD40L was an artifact of decreased activation in the CD40LΔ5 T cells. CD69, however, follows a different activation profile from CD40L, with highest expression at around 6h while the CD40L expression was higher at later time points of 12 and 24h. CD4+ T cells were isolated from dissociated splenocytes from wild type and CD40LΔ5 mice by negative selection, and activated *in vitro* with plate-bound αCD3 with soluble αCD28 mAb for 0 h, 6 h, 12 h and 24 h. Following activation, the CD69 surface expression was studied by flow cytometry. There was no significant change in the CD69 expression in the CD40LΔ5 mice when compared to the wild type (**Figure I-4**).

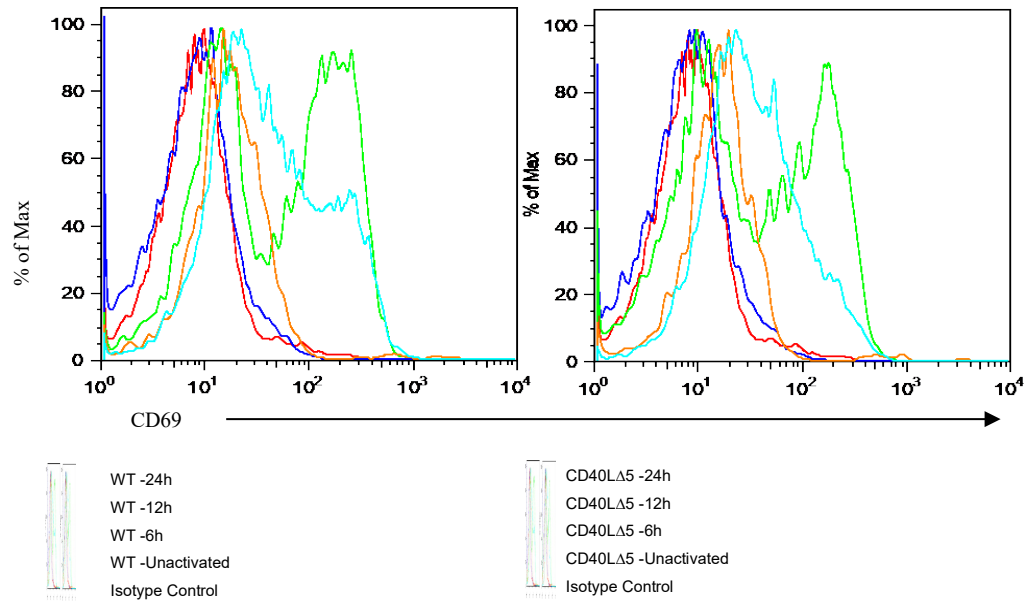

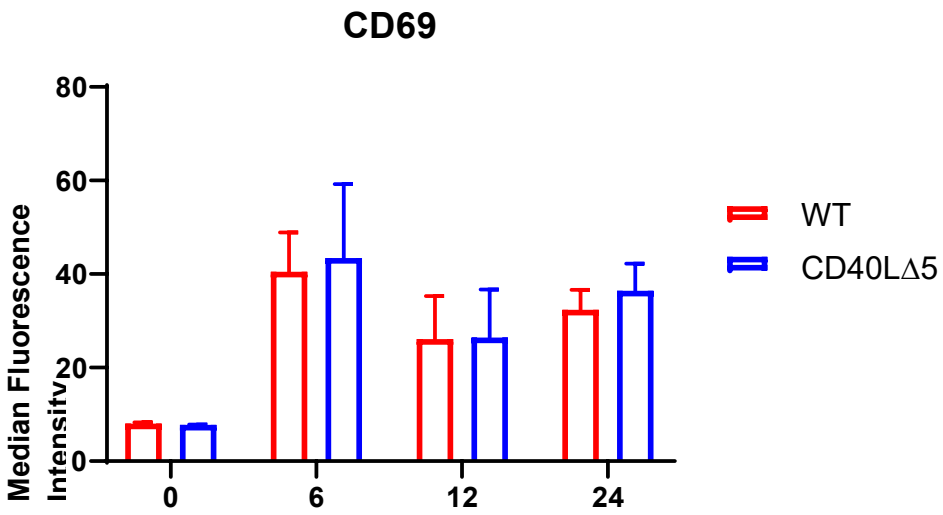

Figure I-4 Activation marker CD69 over a time course of CD4 cell activation. Splenic CD4+ T cells isolated by negative selection were activated *in vitro* with plate-bound αCD3 with soluble αCD28 mAb for different lengths of time (0 h, 6 h, 12 h, 24 h). CD69 expression was measured by flow cytometry using FITC labeled anti-mouse CD69 antibody. (a) Representative histograms show CD69 expression on naïve WT (left) and CD40LΔ5 (right) CD4 T cells activated *ex vivo* as described above. (b) Quantitation of mean fluorescence intensity of CD69 at 0, 6, 12 and 24 h. Data represented as mean+/- SEM of 3 experiments.

Naïve CD40LΔ5 mice have similar immunophenotype as the WT

We evaluated whether the mRNA stability pathway could impact the immune repertoire in naïve mice. Since the Δ5 deletion is in the 3' UTR and there are no mutations in the translated region of CD40L, the question was whether the pre-immunization naïve T cell subsets could be impacted by this mutation. We evaluated the dissociated thymii and spleens by flow cytometry to assess whether prior to antigen challenge either CD4 or CD8 phenotype is preferentially favored in the CD40LΔ5 mice. The CD4/CD8 ratio as depicted shows no significant difference between the wild type and mutant mice in the thymus (top panel) or spleen (bottom panel) (**Figure I-5**a). Furthermore, the major splenic lymphocytic populations CD3 representing the T cells and CD45RB(B220) representing the B cells were compared in the wild type and mutant mice. No significant differences in CD3/CD45RB ratios were observed between the wild type and mutant mice (**Figure I-5**b). In addition, we evaluated the different B cell subsets marginal zone (MZ, B220+,CD23-,$CD21^{hi}$, IgM^{hi}, IgD^{lo}), transitional 1 (T1, B220+,$CD23^{lo}$,$CD21^{low}$, IgM^{hi}, IgD^{lo}) and transitional 2 (T2, B220+,$CD23^{hi}$,$CD21^{lo}$, IgM^{hi}, IgD^{high}) and no significant differences in the distribution of the subsets was observed (**Figure I-5**c). We also compared the thymic CD4, CD8 populations and splenic CD4, CD8, CD3, B220 and CD11b (monocyte/macrophage) populations. Over all there was no significant difference in the immunophenotypic populations in the thymus and spleens of the WT and the CD40LΔ5 mice (**Figure I-5**d).

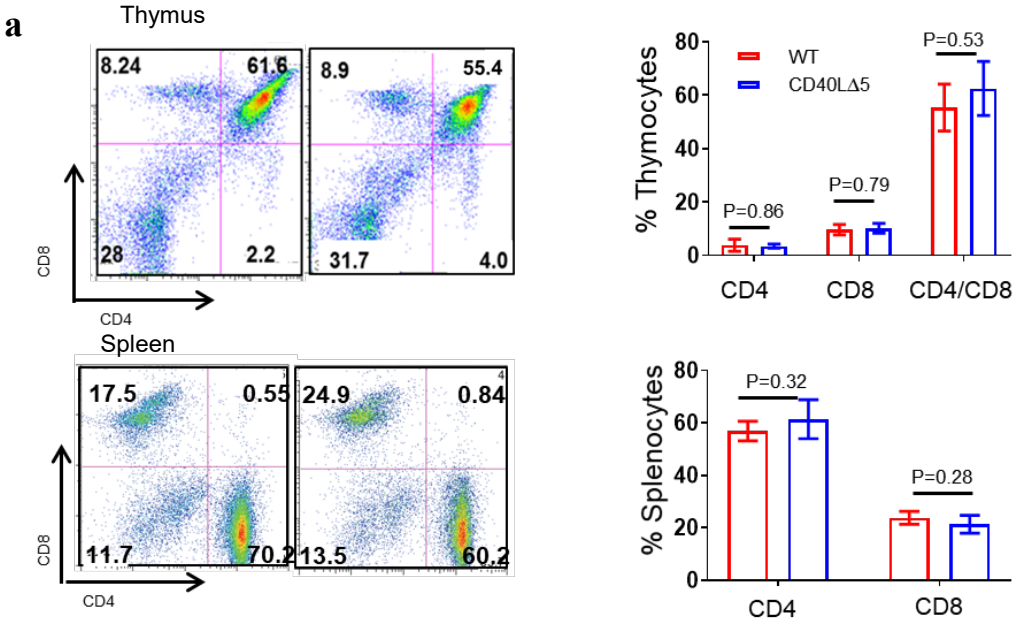
a
Thymus
8.24
61.6
28
2.2
8.9
55.4
31.7
4.0
CD8
CD4
Spleen
17.5
0.55
11.7
70.2
24.9
0.84
13.5
60.2
CD8
CD4
% Thymocytes
WT
CD40LΔ5
P=0.86
P=0.79
P=0.53
CD4
CD8
CD4/CD8
% Splenocytes
P=0.32
P=0.28
CD4
CD8

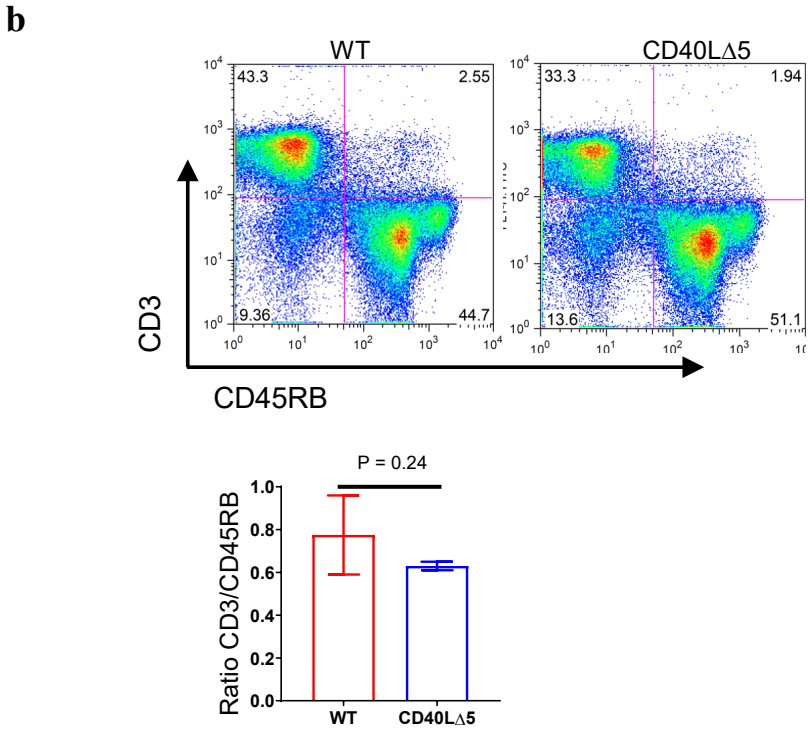
b
WT
CD40LΔ5
43.3
2.55
9.36
44.7
33.3
1.94
13.6
51.1
CD3
CD45RB
P = 0.24
Ratio CD3/CD45RB
1.0
0.8
0.6
0.4
0.2
0.0
WT
CD40LΔ5

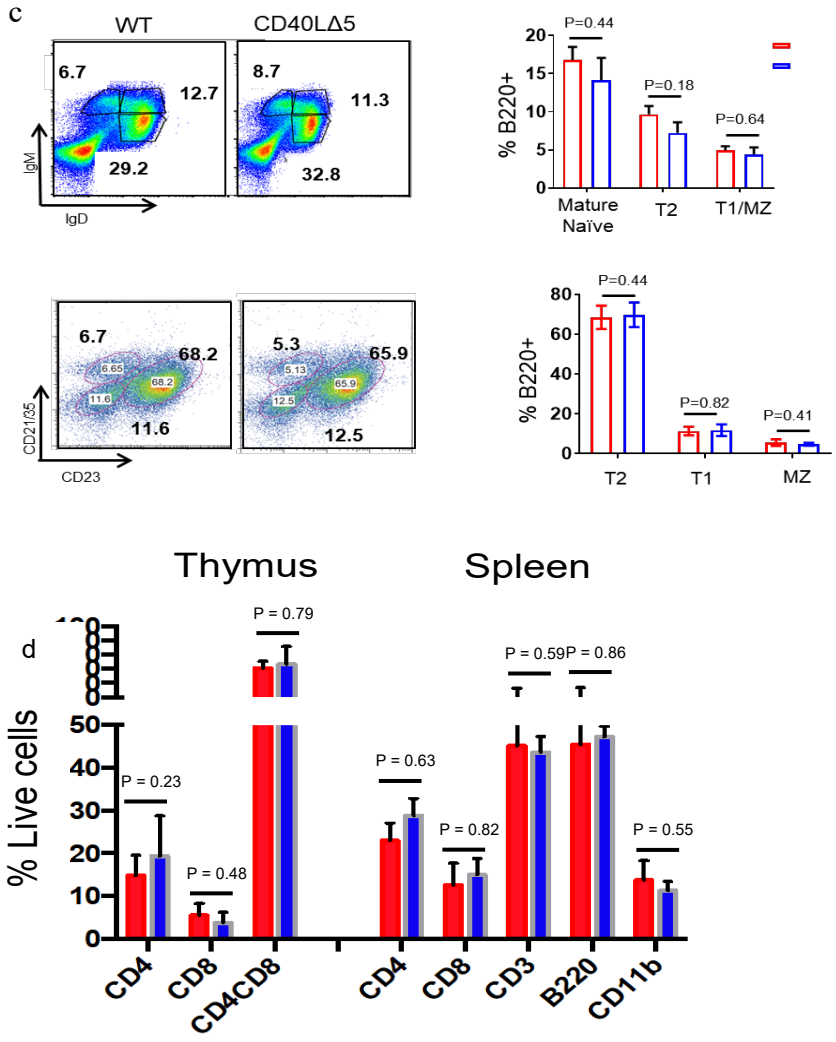

Figure I-5 Immunophenotyping of the dissociated splenocytes from naïve CD40LΔ5 mutant and wildtype mice.

Spleens and thymus were collected from 6-10-week-old mice, dissociated and analyzed for B and T cell population distribution. (a) CD4 and CD8 populations thymus (top panels) and spleen (bottom panels). Histograms (right) showing the Mean/SEM from n=3 experiments. (b) Representative image shows flow cytometry of splenocytes with CD3 (T cells) and CD45RB (B cells). Quantitation of results showing CD3/CD45RB ratio (histogram below) from n=3 experiments. (c) Splenic MZ, ($B220^{+}$, IgM^{hi}, IgD^{lo}, top panel) and ($B220^{+}$, $CD23^{-}/CD21^{hi}$, bottom panel), T1, B220+, IgM^{lo}, IgD^{hi}, top panel) and ($B220^{+}$, $CD23^{lo}/CD21^{lo}$, bottom panel), T2, (B220+, IgM^{hi}, IgD^{hi}, top panel) and ($B220^{+}$, $CD23^{hi}/CD21^{lo}$, bottom panel), in WT and CD40LΔ5 mice (representative plots from 4 independent experiments) and bar graphs showing Mean+/-SEM of the same (right). (d) Thymic CD4, CD8 populations and splenic CD4, CD8, CD3, B220 and CD11b populations in WT (solid red bar) and CD40LΔ5 (solid blue bar). Data shows mean +/- SEM

Target gene	NCBI reference	Forward primer	Reverse primer	Size (bp)
CD40L genomic PCR	NM_011616	tttcactgaccagacttccatctc	gttatgtcccgttgacctgggc	WT-691 CD40LΔ5-507
CD40L	NM_011616	acgttgtaagcgaagccaac	tatcctttcttggcccactg	60
B2M	NM_007393	taacacagttccacccgcctca	gctcggccatactgtcatgctt	188
GAPDH	NM_008084	catggccttccgtgttccta	cctgcttcaccaccttcttgat	103
CD69	NM_001033122	ggtctgggaggtgcgtgtcc	cgtcatctggagggcttgctg	97
CD25	NM_008367	tgtgtctagggtctgcgcca	agcgcttagagtggcctgct	90

Table I-1:Primer sequences

Discussion:

The CD40L knock out mice developed over 30 years ago defined our understanding of the impact of CD40L helper function in the generation of a humoral immune response [42, 85, 86]. While it is well accepted that the immune response is severely debilitated in the absence of CD40L, very less is understood as to how the dynamics of the surface expression of this molecule can affect T cells and their cognate B cells. Here we strive to validate the importance of the mRNA stability element in regulating CD40L expression and whether decreased levels of CD40L affect the development and distribution of immune subsets prior to initiation of the immune response.

Since CD40L surface expression is induced upon activation we stimulated the isolated CD4 T cells *ex vivo* with CD3/CD28 to mimic the TCR specific activation. The decreases in CD40L surface expression in the Δ5 model was obvious only after 24 h of *ex-vivo* activation. This corroborates our previous data that the deletion in the stability element impacts late stage activation CD40L expression [37]. Furthermore, we confirmed, by ex-vivo activation of naïve mouse CD4 T cells followed by evaluation of mRNA stability, that there was indeed an increase in rate of degradation of the CD40LΔ5 mRNA when compared to the wild type. CD69 is a well-established marker for activation in T cells [112, 113]. When we evaluated the CD69 expression in the WT vs CD40LΔ5 mice no differences were observed, indicating that the reduce CD40L expression is not an artifact of reduced activation. This data gives us confidence that the activation induced mRNA stability pathway for CD40L is disrupted in the CD40LΔ5 mice.

CD40L has been shown to be essential for normal development of CD4 T cells. CD40L knockout mice were able to generate effective LCMV specific CD8 T cell responses but had 10-fold lower specific CD4 T compared to wild type mice [114]. The CD40LΔ5 mice unlike the CD40L knock out possess activation dependent levels of CD40L, albeit at lower levels. Thus far there has been no studies to our knowledge that evaluated the effects activation dependent kinetics of CD40L on the T and B cell development. Hence, we evaluated whether this model that lacks the mRNA stabilizing pathway for activation induced regulation of CD40L would result in a skewed distribution of CD4 and CD8 cells in either thymii or spleens of the CD40LΔ5 mice. We found this not to be the case and believe that this, at least in part, can be attributed to the fact that prior to immunization the CD40L stabilizing pathway is probably not in play, so there is no difference in the CD40L expression in the WT and CD40LΔ5 mice. Similarly, we found very little change in the distribution of B cell subsets prior to immunization. Overall, there was no change in the splenocyte or thymocyte sub-populations of T and B cells in the CD40LΔ5 mice indicating that prior to immunization the baseline expression of multiple populations is unaltered in the Δ5 mice. Unlike the CD40L knock out mice the CD40LΔ5 model, does express functional CD40L but at a lower level and this could be the reason we are not seeing a huge change in the immune repertoire. In addition, the mRNA stability pathway is active in response to activation, so plausibly the CD40L expression levels are similar to the wild type in the naïve CD40LΔ5 mice.

Based on this data we decided to evaluate the effect of immunization in the CD40LΔ5 mice when compared to the wild type.

Chapter II : Humoral immune response is significantly affected in the CD40LΔ5 mice post antigen challenge

Abstract:

We have previously shown that regulation of CD40L occurs in part through a posttranscriptional mechanism of activation-induced mRNA stability. This pathway is engaged at extended times of activation and is mediated by the binding of a polypyrimidine tract binding protein (PTBP1) complex to the 3'UTR of the CD40L mRNA. *In vitro* data shows that this pathway leads to sustained expression of CD40L on CD4 T cells at a time when overall transcript levels are low. To understand the role of this regulatory pathway on the humoral immune response we engineered a novel knock-in mouse (CD40LΔ5) that lacked the PTBP1 stability element and challenged them with NP-KLH and Sheep Red Blood Cells (SRBCs). After immunization there were significant decreases in T-dependent antibodies (Abs), and these differences were exacerbated with secondary challenge. In contrast, there were no differences in antibody response to a T-independent antigen. The CD40LΔ5 mice displayed significant changes in multiple aspects of the GC response including reduced levels of plasma cells, memory cells and GL7+ B cells. However, there were no observed differences in the number of T_{fh} cells between the CD40LΔ5 and WT mice. Evaluation of GC structure in splenic sections revealed highly disordered GCs in CD40LΔ5 compared to WT and we observed a significant downregulation of proliferation and upregulation of apoptosis in the CD40LΔ5 B cells when compared to the wild type. Based on this data, we hypothesize that the T cell activation-induced stabilization of the CD40L message and the subsequent regulation of surface expression of the protein is critical for development of a robust GC

response and this occurs on one level by directly impacting the structural architecture of the GC.

Introduction

The complexity of the GC reaction is in the delicate fine tuning of each component and the receptors they engage to perpetrate the reaction. The cascade of interactions and cytokine level control in the GCs result in the development of long-lived plasma cells and memory B cells with high affinity which can ward off attacks from subsequent infections from the same or similar pathogens [58, 102, 115, 116]. GC cell dynamics is orchestrated by a number of cell types from FDCs to T_{fh} and T_{fr} [115]. CD40L expressed on the surface of T_{fh} has been long known to be one of the critical signals for an effective GC response. The elimination of CD40L signal has severe impact on SHM, CSR and plasma and memory differentiation [42, 85, 86]. However, in the CD40LΔ5 model, CD40L is present albeit at a lower level and the expression is activation dependent. Here we attempt to understand the effect of the activation induced mRNA stability pathway and the consequent alleviated expression of CD40L on the different aspects of the humoral immune response.

B cells that recognize their cognate antigen either bind soluble antigen or antigen presented on the surface of antigen presenting cells [117, 118]. The activated B cells upregulate CCR7 a chemokine receptor, that aids the migration of B cells towards the T cell zone [119]. CD40L expression on CD4 T cells is essential for the activated B cells to effectively interact with their cognate T cells at the T cell-B cell border. Once they receive the required signals from the T helper cells, the B cells proliferate at the boundary of the follicle then either seed GCs or differentiate into short-lived extrafollicular (EF)

plasma cells or memory B cells [120, 121]. The initial release of antibodies against the invading antigen is from the EF plasma cells. These B cells are short lived and undergo apoptosis within a few days [122].

The GC B precursors that seed the GCs, proliferate and undergo clonal expansion and the GC develops compartmentalization into the DZ and the LZ. Rapidly dividing centroblasts in the DZ express the chemokine receptor CXCR4 and undergo SHM [46, 58, 60, 115, 123]. CXCL12 the ligand for CXCR4, is secreted by CXCL12-expressing reticular cells, CRCs, are localized in the DZ. thus creating polarity and DZ localization [115, 123]. After each round of SHM in the DZ, the centroblasts downregulate CXCR4, upregulate CXCR5 and drift to the LZ where the FDCs secrete CXCL13 ligand for CXCR5 [58, 60]. It is in the LZ that the centrocytes encounter T_{fh} cells. The CD40L signal is crucial for the interaction of the GC B cells with the T_{fh}. If sufficient CD40L is not available, the T_{fh}/GC-B interaction would be sub-optimal, and the B cells undergo apoptosis. Our model expresses functional CD40L at initial stages of the immune response but shows reduced CD40L resulting from a faster rate of mRNA decay as the reaction progresses. Although with our model we are limited in our ability to follow the reaction in real-time, we find that sufficient CD40L is available for the B cells to initiate GCs but as the reaction proceeds the T_{fh} have decreased CD40L for interactions with the GC B cells and subsequently GC B cells do not receive sufficient T_{fh} help.

If sufficient CD40L signal is present, the B cells move back into the DZ for further affinity maturation or differentiate into high affinity plasma cells. Somatic hypermutation (SHM) of immunoglobulin variable region (IgV) genes leads to affinity maturation and is one of the critical components of the GC reaction in T dependent

responses[124, 125]. T_{fh} help with sufficient CD40L is essential to ensure proper selection of GC B cell clones carrying affinity enhancing mutations. Although the GC reaction was believed to be essential for SHM, in recent years SHM has been shown to occur in the absence of or prior to the formation of GCs [69, 126]. Salmonella Typhi infection for example is characterized by extensive extra-follicular plasma cell response with a delayed GC formation which show extensive SHM and class switching [127].

In the GCs, if the CD40/CD40L interaction is effective the GC B cells receive directions to either migrate back into the DZ for further expansion and fine tuning affinity enhancing mutations or proceed to a plasma or memory differentiation path [50, 58]. This cycle of somatic hypermutation and clonal selection allows the B clones mutated to express the higher affinity BCRs, to be preferentially selected while lower affinity clones either leave the GC as memory B cells or undergo apoptosis [128]. Affinity maturation is significantly reduced in CD40L knock out mice [42, 86]. In a scenario where SHM is not impaired, the B cell clones would then interact with the T_{fh} for selection and conceivably, if CD40L is reduced at this stage, the interaction will not be effective. This in turn would lead to lower titers of high affinity antibodies.

Memory B cells initiate after the crucial decision for differentiation of GC B cells is made based on interaction with the T_{fh} cells in the LZ of the GC. IgG and IgM memory B cells are different in that the former favors differentiation into plasma cells, while the latter primarily seeds GCs [59]. Memory B cells have been shown to differentiate from activated precursor cells expressing CD38 and GL7. The CD40/CD40L signal alone can induce production of activated memory B cells but not GC B cells [99, 101]. CD40L knock out mice have severely impaired memory responses [87].

The activated B cell modulates the antibody heavy chain while keeping the complementarity determining regions for antigen specificity unmodified by a process called class switch recombination (CSR). The primary response, the V-D-J region transcribed with a Cμ gene is processed to produce the IgM transcript. As the B cell matures after interaction with the Th cells, the Cγ is aligned against the same V-D-J combination, while the sequences are cleaved off at switch regions, releasing switch circles. The transcript after processing generates mRNA coding for the IgG heavy chain. CSR is largely thought to be CD40L dependent, however studies have shown CSR to be stimulated by viral glycoproteins and lipopolysaccharide from gram-negative bacteria in a CD40L independent manner [74, 129, 130]. In mice infected with Citrobacter rodentium, basal serum isotype levels were similar for IgM and IgG3 but total IgG and IgG2b were significantly lower and IgG1 and IgG2c levels were undetectable [112]. Primary IgG1 response to lymphocytic choriomeningitis virus (LCMV) was severely impaired in the CD40L knock out mice [87].

Our lab has established that CD40L mRNA stability in mouse CD4 cells is activation-induced and regulated by the interaction of protein complexes with highly specific elements within the CD40L 3'UTR that regulate the stability of the transcript and influence its localization within the cell [110]. In this study, we strive to understand how the effect of *in vitro* deletion of part of the 3'UTR PTBP1 complex binding stability element of CD40L impacts CD40L expression *in vivo* with the CD40LΔ5 model.

Materials and Methods

Mice:

C57BL6/J mice were obtained from Jackson Laboratories. CD40LΔ5 mutant was generated deleting the PTB containing complex binding sites B and C (Δ5) in the 3'UTR sequences between 900 -1086, by site-directed mutagenesis. The neomycin-resistance gene (Neo_r) was removed by crossing the mice carrying the targeted allele to Cre-deletor transgenic male. The resultant mice carrying the Cre were backcrossed to the C57BL/6 WT multiple rounds to remove the Cre.

Immunization:

The haptan antigens, 4-hydroxy-3-nitrophenyl-acetyl conjugated to Keyhole Limpet Hemocyanin (NP-KLH) and 4-Hydroxy-3-nitrophenylacetic (NP) hapten conjugated to aminoethyl carboxymethyl-FICOLL (NP-AECM-FICOLL) were dissolved in sterile PBS at a concentration of 1 mg/mL. For primary immunizations, NP-KLH or NP-AECM-FICOLL were mixed with Alum at a 1:1 ratio and 200 µL containing 100 µg of NP-KLH or NP-AECM-FICOLL was injected interperitoneally (i.p.) into mice using a $25G_{5/8\text{-gauge}}$ needle. At days -4, 7, 14, 21 and 28, blood was collected by submandibular bleeding, spun down and serum collected. Spleen and bone marrow samples were collected from NP-immunized and boosted (Day 21) mice at day 28. To test the T-dependent polyclonal antigen, SRBCs (Innovative Research Inc., Novi, MI) were resuspended at a ratio of 1:1 in PBS and 100 µl was injected i.p. Mouse spleens and bone marrows were harvested 8 days after injection. Splenic or bone marrow mononuclear cells were dissociated mincing the spleen between glass slides, filtered using a 40-µm Falcon cell strainer and suspended in 1X HBSS with 5% FBS. Bone marrow cells were isolated by flushing the femurs with

PBS. Dissociated spleens were subject to RBC lysis. Following RBC lysis for 35 seconds using 1X ACK lysis buffer, the cells were washed 3X with HBSS containing 5% FBS and resuspended in RPMI with 10% FBS and counted.

Antibody titer determination by ELISA:

Nunc maxisorb, 96-well plates were coated with 50 µL per well of 5 µg/mL of NP8-BSA or NP25-BSA diluted in PBS. Two rows of each plate were coated with 2.5 µg/mL capture antibody diluted in carbonate-bicarbonate buffer (pH 9.6) to generate a standard curve. The plates were sealed with parafilm and incubated overnight at 4^0 C. The following morning plates were washed 3X with 200 µL each of wash buffer, 1X Phosphate Buffered Saline with 0.1% Tween 20 (1X PBST). To block non-specific binding, PBS containing 2% BSA was added to the plates and incubated at room temperature for 1 h. The sample dilutions were added to the plates (50 µL) and incubated for 2 h at 37^0c. At the end of the incubation the plates were washed 3 times in wash buffer and blotted dry. Detection antibody was diluted 1:2000 in PBS–1% BSA and 50 uL was added to each well and incubated at room temperature for 1 hour. The plates were washed 4X with wash buffer, blotted dry and 50 µL of freshly prepared PNPP substrate solution was added to each well. After 10-30 min incubation at RT the plates were read on a spectrophotometer at 405 nm absorbance. The standard curves were plotted using GraphPad Prism and the concentration of the samples interpolated from them.

Elispot detection of NP-specific ASCs:

Each well of a filtration plate was pre-wet with 15 µL of 35% ethanol for 1 minute followed by 3 washes with 200 µL of sterile PBS. The plates were coated with 100 µL of NP-BSA at a concentration of 50 µg/mL in sterile PBS and incubated at 4^0C overnight.

The plates were blocked with 100 µL per well of culture medium (RPMI with 10% FBS) for 2 h at 37^0C followed by washing 6X with 1X PBST. Two-fold dilutions of cells starting from 1E6 cells per 100 µL were prepared and added to the Elispot plate and samples incubated overnight at 37^0C/5% CO2, followed by washing 6 times with 1X PBST. 100 µL of AP-conjugated anti-mouse IgG1 (1:2000 in PBS + 2% BSA) was added to the plate and incubated at RT for 1 h. The plate was washed 3X with 1X PBST and 3X with PBS. Ready to use NBT/BCIP substrate buffer was added at 100 µL per well and incubated 5–10 min. Spot development was stopped by washing under running water. The plate was blotted and left it to dry overnight under the hood in the dark and spots counted.

Flow Cytometric immunophenotyping post antigen challenge:

Dissociated splenocytes and bone marrow cells were stained with Zombie-NIR fixable viability dye (Biolegend) for 15 min washed and then stained for surface antigens. To stain the lymphocytes for flow analysis, 1×10^6 cells were suspended in PBS with 1% BSA and 2% rat serum with 1µg/mL of 2.4G2 (anti-FcγR) to block FcR binding. After 10 min of incubation on ice, the appropriate primary antibodies were added to the cells at 1-10 µg/mL depending on the manufacturer's recommendation and incubated for half an hour on ice. The cells were then washed twice with PBS containing 1% BSA, and secondary antibodies were added where necessary for another 30 min on ice. The cells washed twice in PBS were resuspended in 1% paraformaldehyde in PBS fixative. For intra-cellular antigens the fixed cells were either incubated with 0.1% Triton-X for 5 min and washed twice before staining or maintained in Cytofix/Perm buffer (BD) for the

duration of staining. Flow cytometric analysis was performed on a FACS Calibur or Cytek Northern Lights cytometer. The list of antibodies used is included in the Table II-1.

Isolation of total B cells and GC B cells:

Mouse B cells were isolated from splenocytes using MojoSort CD19 positive selection kit. 10µL of CD19 nanobeads were added to 10^7 mixed well and incubated on ice for 15 min. At the end of the incubation 2.5mL of MojoSort buffer was added and the tube placed in the magnet for 5 min. The unlabeled fraction was poured off and the beads washed 1X in PBS. The steps were repeated two more times to remove any remaining non- B cell fraction. So as to isolate the GC B cells, we used GC B Cell (PNA) MicroBead Kit (Catalog# 130-110-479, Miltenyi Biotec). 10 µL of PNA-Biotin was added per 10^7 total cells, incubated for 5 min on ice followed by addition of 20 µL of anti-Biotin MicroBeads and incubation for an additional 10 min. Cells were then washed and resuspend in 500 µL of buffer and applied to a magnetic separation column and bound cells collected after removal from the magnet.

Sequencing of V186.2 gene rearrangement:

The isolated GC B cells were incubated for 10 min at room temperature in 800 µL Trizol, passed two times through a 26½G needle using a 1 ml syringe to shear the DNA, 200 µL chloroform was added and shaken vigorously with hand for 15 s. Following 3-minute incubation at room temperature, the samples were centrifuged at 4^0C for 15 min at 12000 Xg. The upper layer of the interface was transferred to a new tube and precipitated with 400 µL isopropanol for 10 min at RT followed by pelleting with centrifugation. The pellet was washed with 1 ml 75% ethanol in DEPC-treated water and dried on the bench for 15 min. The RNA was resuspended in 7 µL DEPC-treated water. So as to selectively

amplify V186.2 Cγ1-membrane transcripts, RNA was reverse-transcribed using an oligonucleotide hybridizing in the Cγ1-membrane-encoding exon (5'-TGACAGCAGCGCTGTAGCAC-3'). 2 µL of cDNA was added to a master mix consisting of 8 µL dNTP solution (1.25 mM), 5 µL 10X PCR reaction buffer, 5 µL MgCl2 (25 mM), 1 µL V186.2-leader primer (5'-CATGCTCTTCTTGGCAGCAACAG-3'), 1 µL Cγ1- membrane-encoding exon (mCγ1-PCR oligo: 5'-CAGCACAGGTCTCGTCCAGTTG-3'), and 27.5 µL H2O and amplified for 30 cycles with the amplification conditions 95^{0}C 2 min, 30X (95^{0}C 30 s, 70 ^{0}C 30 s, 72 ^{0}C, 90 s), 72 ^{0}C 5 min, and 10 ^{0}C pause. The PCR band was isolated from an agarose gel, using QIAquick Gel Extraction kit (Qiagen). The PCR product was ligated into the pGEM-T Easy vector using the following protocol. The PCR product was added to 1 µL of 10X PCR reaction buffer, 0.8 µL MgCl2 (25 mM), 1.6 µL dNTPs (1.25 mM), and 0.2 µL Taq polymerase mixed and incubated for 20 min at 70 ^{0}C, placed on ice. For the ligation reaction using the pGEM-T Easy vector kit 5 µL ligation buffer, 0.5 µL cloning vector and 2 µL of PCR product, 1.5 µL H2O, and 1 µL T4 ligase were added mixed and incubated for 1 hour at room temperature. 2 µL of the ligation reaction was added to 50 µL DH5α competent bacteria and following heat shock, 500 µL SOC medium was added and the bacteria allowed to grow for 1 h at 37 ^{0}C. 100 µL of culture was spread onto an agar plate containing ampicillin. The colonies were transferred into 40 µL of H_2O, vortexed and 3 µL added to a master mix containing of 28.5 µL H2O, 8 µL dNTP solution (1.25 mM), 5 µL 10X PCR reaction buffer, 3 µL MgCl2 (25 mM), 1 µL V186.2-nested primer, 1 µL Cγ1-PCR primer (for PCR primers, see Table 1), and 0.4 µL Taq polymerase. The PCR program was run as follows, 95 ^{0}C 2 min, 32X (95 ^{0}C 30 s, 70 ^{0}C

30 s, 72 ^{0}C 90 s), 72 ^{0}C 5 min, and 10 ^{0}C pause. Samples were sequenced with the T7 primer. The sequence was run against the VBASE2 database (V186.2 corresponds to musIGHV057). The V186.2 mutation frequency was determined dividing the number of somatic mutations by the number of V186.2 nucleotides sequenced, excluding N, D, and joining (J) sequences.

Immunohistochemistry:

Spleens from NP-KLH or SRBC-immunized mice were embedded and snap frozen in Optimal Cutting Temperature compound (OCT, Sakura Fintech, Torrance, CA) and stored at -80°C. 20µm sections were cut on a Leica CM1900 cryostat microtome (Leica, Germany), air dried for 10 min, fixed in acetone at -20°C for 5 min. After rehydration with 1X PBS, sections were then blocked with 1x PBST containing Fc-block and 3% BSA. For staining the sections, anti-CD4 –Alexafluor-594 (RM4-5, BioLegend), anti-IgD –APC (allophycoerythrin) (IA6-2, BioLegend) and anti-GL7-Alexafluor-488 (Biolegend) were added to PBST with 1% Fc Block. After 1 hour the sections were washed with PBST and mounted using Prolong Gold mounting media. Stained sections were visualized using a Nikon Eclipse E600 fluorescence microscope with a XM-20 digital color camera or Zeiss LSM850 confocal microscope and processed using Adobe Photoshop. 16 images were collected at 10X magnification from wild type and CD40LΔ5 mice and the number of GCs per image calculated. The GCs were identified using Olympus Studio 2 software and the number of GC per image frame calculated. The area of each individual GC was also quantitated using the same software and the GC area between WT and CD40LΔ5 mice was compared.

RNA Seq Transciptome analysis:

The DNA library for RNA-seq analysis was constructed with an NEBNext Ultra RNA Library Prep Kit for Illumina (NEB) by Novogene. The size range of the resulting DNA library was estimated on a 2100 Bioanalyzer (Agilent Technologies). After checking the molar concentration by qPCR, the DNA library was subjected to sequencing on a HiSeq 1500 sequencer (Illumina) in a 49-bp single-end read mode. The raw data were processed with CASAVA 1.8.2 (Illumina) to generate fastq files. The sequence reads were aligned to the Mus musculus reference genome (mm9) using STAR. According to the mapped data, the fragments per kilobase of exon per million reads (FPKM) was calculated with the M. musculus genome annotation NCBI build 37.2. The differential expression analysis of two conditions/groups was performed using the DESeq2 R package. The resulting P values were adjusted using the Benjamini and Hochberg's approach for controlling the false discovery rate. Three biological replicates were used for each population. To identify biological functions or pathways are significantly associated with differential expressed genes, the clusterProfiler software was used for enrichment analysis, including Gene Ontology (GO), KEGG and Reactome database Enrichment. GO, Reactome and KEGG terms with padj < 0.05 are classified as significant enrichment.

Results

CD40LΔ5 mutation results in decreased CD40L expression

Since, the Δ5 deletion is in the 3'UTR of the CD40L mRNA and the CD40L translated protein is unaffected by this mutation, the CD40LΔ5 mice should be able to express normal levels of CD40L and be able to initiate the early interaction with B cells. *In vitro* data from our lab, has shown that at later stages of activation, the decrease in surface CD40L is a consequence of the reduced stability and hence faster decay of the CD40L mRNA. The first question we asked was whether *in vivo* stimulated CD4 cells from the CD40LΔ5 mice show a decrease in surface CD40L expression when compared to the wild type. Due to the constrains of regulating the time points of activation *in vivo*, we used an *ex vivo* activation system with re-stimulation using KLH, after initial antigen challenge and booster with NP-KLH.

Draining mesenteric lymph node from CD40LΔ5 and WT littermates immunized and boosted (21 days) with NP-KLH were collected (Day 28) and dissociated. The total lymphocytes were incubated for different periods of time (0, 6, 12 and 24h) in the presence of KLH and subject to flow cytometric analysis. The principle behind this experiment was to allow APCs to present the antigen to the KLH-specific CD4 T cells and hence bring about activation which would in turn increase the expression of CD40L in these cells. When we evaluated the CD4 gated cells by flow cytometry we found that these cells expressed CD40L both prior to (due to *in vivo* priming) and post *ex vivo* stimulation but there was an exponential increase in expression after re-stimulation. When compared to the wild type, the CD40LΔ5 mutant had significantly lower surface expression of CD40L before and after the *ex vivo* KLH exposure (**Figure II-1**a, left) At

the 12h timepoint of *ex vivo* activation there was a significant decrease in the CD40L expression in the CD40LΔ5 when compared to the wild type (**Figure II-1**a, right). Evaluation of the kinetics of CD40L surface expression over a 24-hour time course of *ex vivo* activation indicated that the effect of the CD40LΔ5 deletion was significant only at 12 h after KLH re-exposure (**Figure II-1**b).

To confirm that the decrease in surface expression corresponded to a decrease in mRNA stability, we assessed the mRNA decay rate of the CD40L in CD4 T cells from CD40LΔ5 mice relative to the wild type. RNA was extracted from samples stimulated 12 h *ex vivo* with KLH and the amount of RNA remaining after incubation with DRB for 1.5 h was quantitated. We observed that CD40L mRNA decay was more accelerated in the CD40LΔ5 than in the wild type (**Figure II-1**c). Since the expression of CD40L is directly correlated to activation we evaluated two additional activation markers, CD69 and CD25, to confirm that the changes in CD40L expression are not a consequence of reduced CD4 T cell activation in the CD40LΔ5 mice. Evaluation of CD69 and CD25 by flow and qPCR indicated that there was no significant difference in the levels of CD69 and CD25 between the CD40LΔ5 and wild type mice (**Figure II-1**d,e).

To understand the *in vivo* kinetics of CD40L expression we collected splenocytes from CD40LΔ5 and wild type mice at day 0, 2, 4 and 8 post immunization with SRBCs and evaluated CD4+CXCR5+PD-1+ T_{fh} cells for CD40L expression by flow cytometry. We discovered that the CD40L expression in the CD40LΔ5 mice was comparable to that of the wild type at early stages of the immune response, namely 2 and 4 day with a significant decrease by day 8 (**Figure II-1**f).

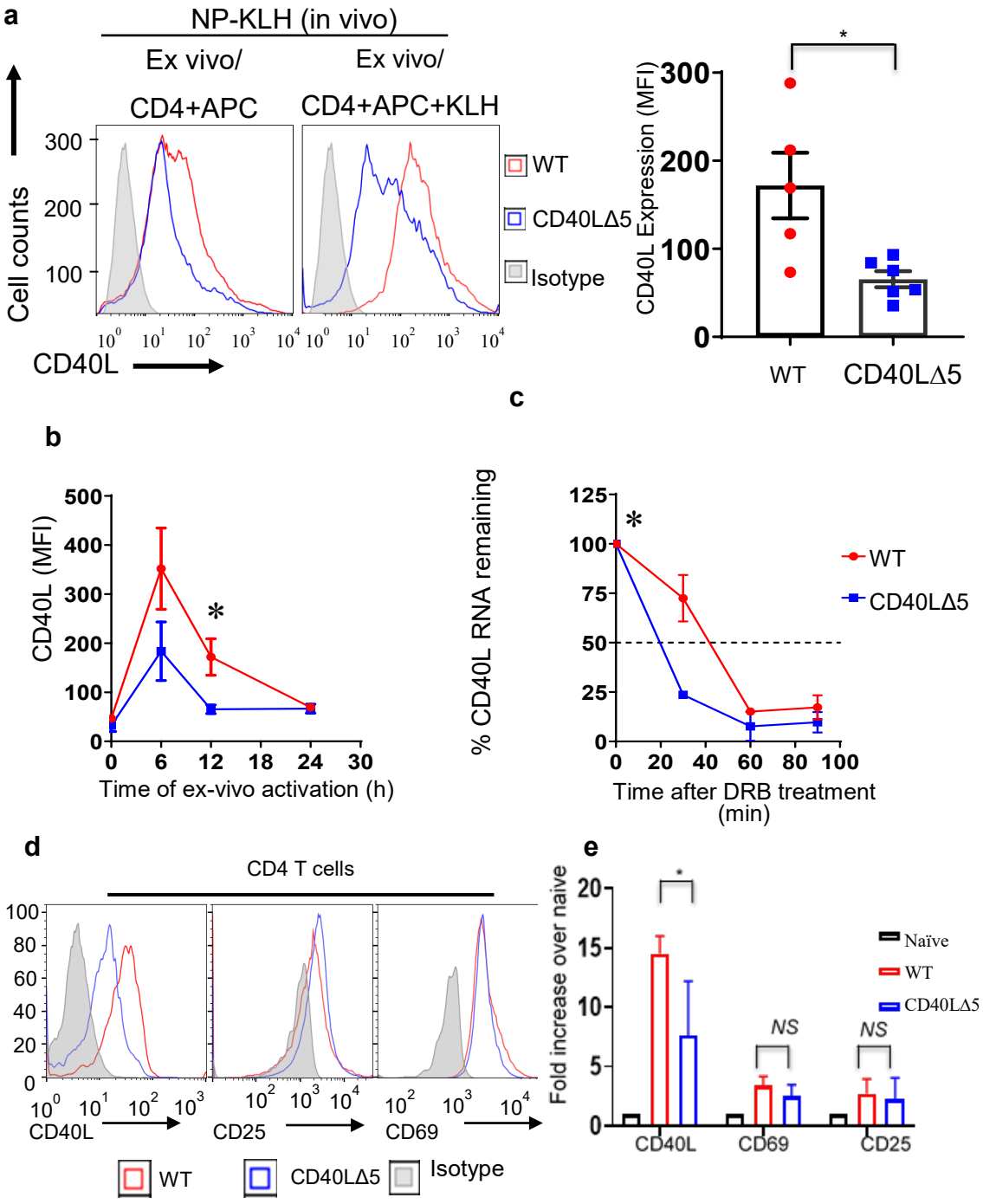
a
NP-KLH (in vivo)
Ex vivo/
CD4+APC
Ex vivo/
CD4+APC+KLH
Cell counts
CD40L
WT
CD40LΔ5
Isotype
CD40L Expression (MFI)
WT
CD40LΔ5
b
CD40L (MFI)
Time of ex-vivo activation (h)
c
% CD40L RNA remaining
Time after DRB treatment (min)
WT
CD40LΔ5
d
CD4 T cells
CD40L
CD25
CD69
WT
CD40LΔ5
Isotype
e
Fold increase over naive
Naïve
WT
CD40LΔ5
NS
NS
CD40L
CD69
CD25

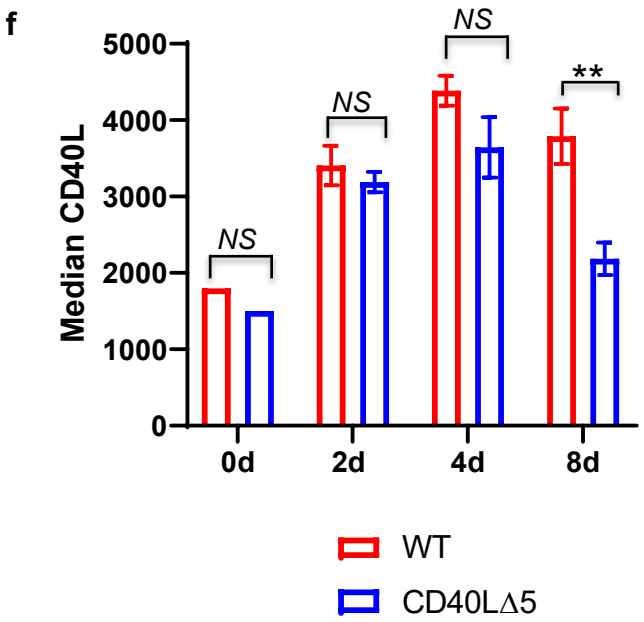

Figure II-1 Decreased surface CD40L and reduced mRNA stability was observed on activated CD4 T cells in CD40LΔ5 mice.
Analysis of CD40L surface expression on wild type and CD40LΔ5 CD4 T cells from draining mesenteric lymph nodes collected on day 28 post immunization (day 0) and booster (day 21) with NP-KLH. Dissociated lymphocytes including T cells and APCs were incubated *ex-vivo* in the presence of KLH for 0,6,12 and 24 h and stained for surface CD40L. (a) Representative plot showing CD40L expression in WT (red), and CD40LΔ5 (blue) relative to the isotype control (solid gray) after 12h ex-vivo activation (left). Quantitative results of surface CD40L expression at 12h post ex vivo activation showing individual mice, WT (red dots) and CD40LΔ5 (blue squares) (right) (b) Expression of CD40L on CD4 gated cells evaluated over the time course of 0,6,12 and 24 h, WT (red) and CD40LΔ5 (blue) (c) Dissociated mesenteric lymph node cells activated *ex-vivo* with KLH, were incubated with DRB over a 1.5 h time course and RNA isolated and evaluated for remaining CD40L normalized to GAPDH expression by qPCR, WT (red) and CD40LΔ5 (blue). (d) CD40L, CD69 and CD25 surface expression on CD4+ cells 12 h post ex vivo activation were evaluated by flow cytometry and (e) RNA levels of CD40L, CD69 and CD25 quantitated by qPCR normalized to GAPDH (depicted as fold increase over naïve), following 12 h *ex vivo* activation with KLH. (f) Dissociated splenocytes from wild type (red) and CD40LΔ5 (blue) gated on CD4+CXCR5+PD-1+ T_{fh} cells evaluated by flow cytometry for CD40L expression over a time course of 0, 2, 4 and 8 days. Results are represented as mean ± SEM. Significance was assessed by student's unpaired t-test where *$p < 0.05$; **, $p < 0.005$; and ***, $p < 0.0005$ was considered significant.

Decreased CD40L mRNA stability leads to a reduced antibody titers and reduced class-switch recombination (CSR)

The consequence of depleting CD40L during an immune response is reduced ability for the CD4 helper cells to provide sufficient help to B cells [131]. The down-stream result of this would be a poor immune response as observed by lowered antibody titers against the antigen. The question we addressed was whether disrupting the activation mediated mRNA stability pathway would impact antibody titers and isotype distribution.

So as to quantitate NP specific serum titers of isotype switched (IgG1, IgG2b, IgG2c) and non-switched (IgM) antibodies, we injected WT and CD40LΔ5 mice with NP-KLH and provided a booster after 21 days. Serum was collected weekly and levels of IgG1, IgG2b, IgG2c, IgG3, IgA and IgM were measured. At all time points tested, significant decreases were observed in the IgG1, IgG2b, IgG2c, primary responses in the CD40LΔ5 mice when compared to the WT (**Figure II-2**a), and the impact was more enhanced in the secondary responses measured at 28 days (**Figure II-2**b). IgM titers were significantly lower only in the secondary response, and IgG3 was unaffected in both the primary and secondary responses (**Figure II-2**a).

IgA and IgE were also evaluated and IgA was not significantly different between WT and mutant and the level of IgE was below detection limit (data not shown). It was also observed that the NP-Ficoll (a T independent antigen) injected mice showed no significant IgG1, IgG2b and IgG2c but a high level of IgG3 which was not significantly different between the wild type and the mutant (data not shown).

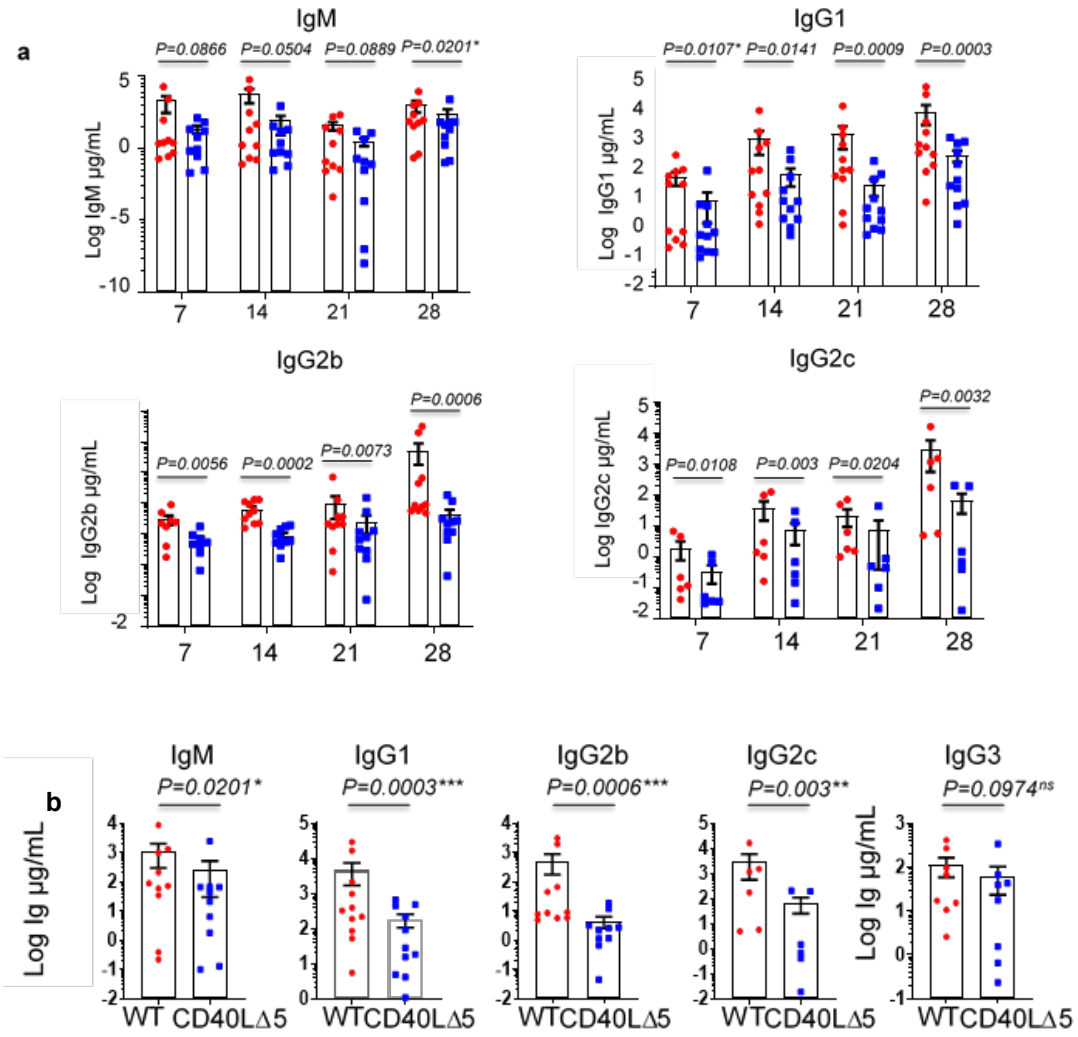

Figure II-2 Reduced T dependent antibody responses in CD40LΔ5 mice.
6-10-week-old WT and CD40LΔ5 mice were injected i.p. with 100 µg NP-KLH (Day 0) and boosted (Day21). (a) ELISA analyses of antibody isotypes performed on sera collected from mice at days 7, 14, 21 and 28 post immunization/boost. (b) The secondary response as measured by serum titers of isotypes 7 days post booster at Day 28. Individual mice represented in graphs with mean +/- SEM of all mice tested. Significance was assessed by student's unpaired t-test where *$p < 0.05$; **, $p < 0.005$; and ***, $p < 0.0005$ was considered significant.

Somatic Hypermutation and affinity maturation are affected in the CD40LΔ5 mice

To evaluate the effect of the deletion on the affinity maturation the IgG1 response to NP_8-BSA was compared to that for NP_{20} -BSA. NP_8 with lower levels of antigen relative to BSA allows for only higher affinity antibodies to bind. The relative NP_8:NP_{20} ratio is a measure of the percentage of antibodies that are high affinity in the serum. The CD40LΔ5 mutant had significantly lower NP_8:NP_{20} ratio compared to the WT only in the secondary response indicating there might be reduced levels of somatic hypermutation at subsequent stages of activation (**Figure II-3**a).

To further determine the level of SHM that was occurring in the mutant and wild-type mice we extracted RNA from isolated PNA positive GC B cells, generated Cγ1 specific cDNA and amplified the V186.2 region by PCR. The V186.2 fragments were then cloned into the pGEM-T vector and individual colonies isolated and sequenced. The immunogen NP coupled to a carrier molecule like KLH leads to the selective enhancement of the IgV heavy chain fragment, V_h186.2. It is also characterized by a somatic mutation in codon 33 of V_h186.2 leading to a tryptophan to leucine amino acid exchange with subsequent increases in the antibody affinity by around 10-fold, marking affinity maturation [132-134]. We, therefore, compared the number of W(tryptophan) to L(Leucine) switched colonies from wild type and CD40LΔ5 mice. We found a significant difference in the number of high affinity mutations in the wild type when compared to the CD40LΔ5 mice. 60% of the wild type and 40% of the CD40LΔ5 colonies carried the W33L mutation (**Figure II-3**b). We also estimated the total number of mutations in the

individual V186.2 region and we didn't observe a significant difference between the wild type and the CD40LΔ5 (**Figure II-3**c).

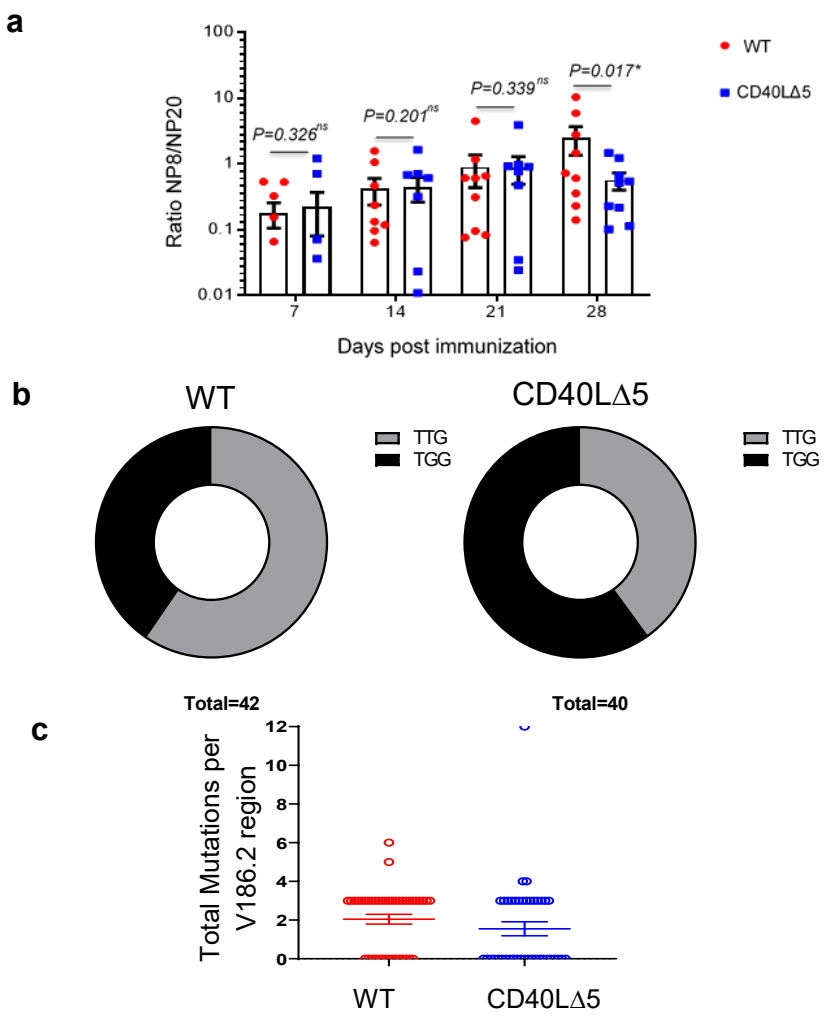

Figure II-3 Rate of SHM is unaffected but affinity maturation is impaired in CD40LΔ5 WT and CD40LΔ5 mice were injected i.p. with 100 ug NP-KLH and boosted on Day 21. ELISA analysis for IgG1 was performed with NP8 and NP20 on sera collected from the mice at days 7, 14, 21 and 28 post immunization/boost. PNA+B cells were isolated from the dissociated splenocytes by positive selection, RNA was isolated, Cγ1 specific cDNA generated and the V186.2 region amplified by PCR. The V186.2 fragments were then cloned into the pGEM-T vector and individual colonies isolated and sequenced. (a) The ratio of relative titers of antibodies against NP8 to that of NP20 was used to assess affinity maturation at 7-, 14-, 21- and 28-days post immunization/boost. (b) Colonies showing TTG (light gray bar) in the codon 33 of V186.2 are considered affinity matured TGG (black bar) represents the unmutated. Data compiled from 42 WT and 40 CD40LΔ5 colonies. (c) The total number of mutations per V186.2 region for WT (red) and CD40L5 (blue) mice. Significance was assessed by student's unpaired t-test where *p < 0.05 was considered significant. Individual mice shown with the mean +/-SEM.

Plasma cell numbers are reduced in the CD40LΔ5

We observed a significant reduction in anti-NP antibody titer in the CD40LΔ5 relative to the wild type for all isotypes tested except IgG3. We needed to evaluate whether the impaired antibody response was a direct consequence of decrease in antibody secreting plasma cells. We tested the effect of the CD40LΔ5 deletion on the number of NP-specific antibody secreting cells (ASCs) by ELISPOT analysis. When NP-KLH challenged and boosted wild type and CD40LΔ5 splenocytes were tested, there was a significantly lower percentage of anti-NP IgG1 plasma cells in the spleen of CD40LΔ5 mice when compared to wild type. We also evaluated the bone marrow ASCs but didn't see a significant difference between the wild type and CD40LΔ5 (**Figure II-4**a, left panel).

Since the bone marrow plasma cells represent the long-lived ASC population, we further determined the long-term responses to NP-KLH immunization by injecting mice with 100µg of NP-KLH and boosting on day 45. At the 180-day timepoint we harvested the mice, collected spleens and bone marrows and evaluated the number of ASCs by ELISPOT. There was a significant decrease in the number of ASCs per million splenocytes in the CD40LΔ5 mice when compared to the WT but as before the number of ASCs in the bone marrow failed to achieve significance. When we compared the number of IgG1+ spots from the spleen and the bone marrow at 180 days, there were significant differences in the spleen, but the bone marrow ASC counts were similar in the CD40LΔ5 and the WT (**Figure II-4**a, right panel). When the number of ASC per million cells were compared at Day 28 vs Day180, the bone marrow had relatively the same number of ASCs (**Figure II-4**b).

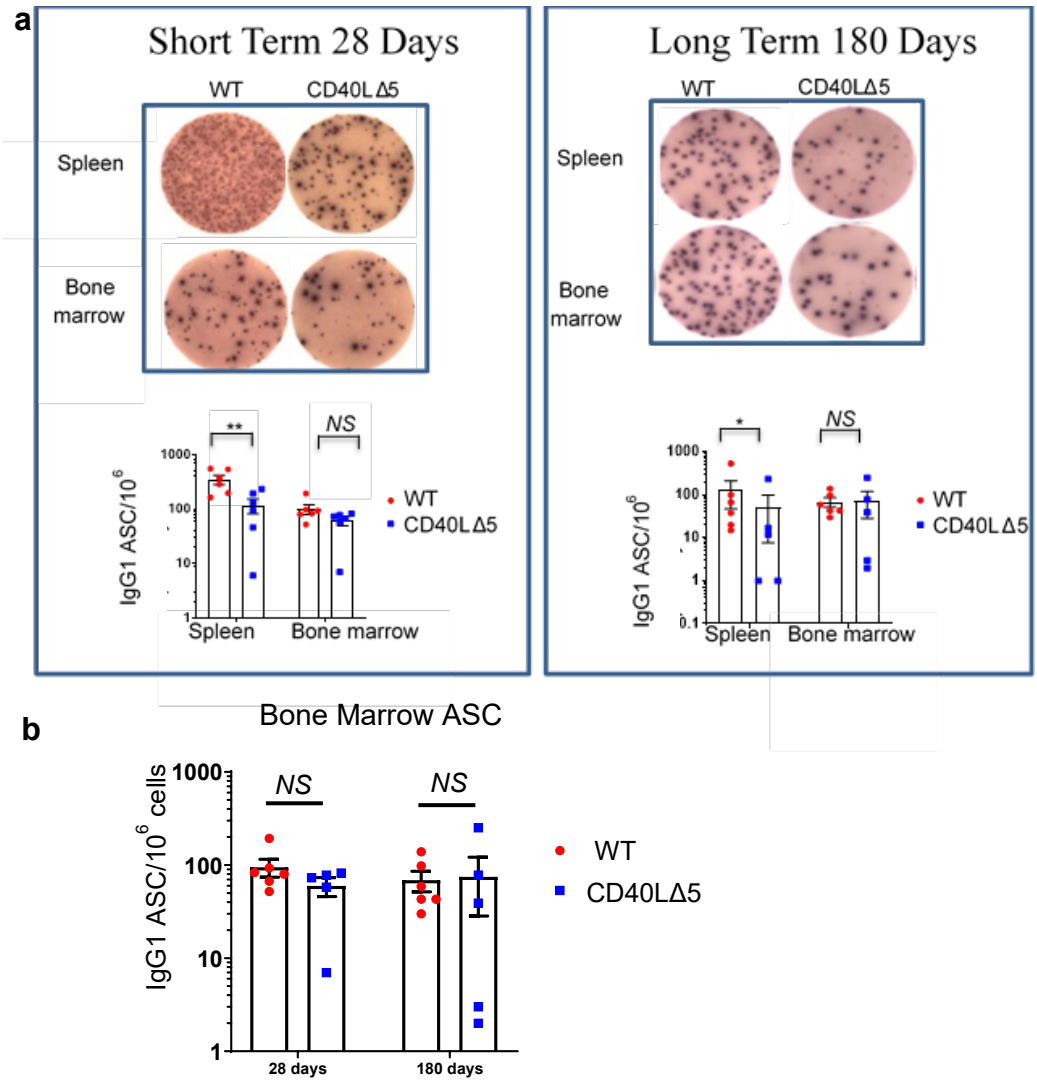

Figure II-4 Decreased number of ASCs observed in the CD40LΔ5 spleen:

WT and CD40LΔ5 mice were injected i.p. with 100 ug NP-KLH and boosted on Day 21 (or Day 45 for long term response). Splenocytes were collected on Day 28, (or Day 180 for long term response), plated on an NP_{20} BSA coated mixed cellulose ester plate and incubated overnight, followed by probing with an anti-IgG1 antibody conjugated to HRP. Spots formed after addition of NBT BCIP substrate, were counted manually (a) Relative number of spots on WT (left) and CD40LΔ5 (right) and spleen (top) and bone marrow (bottom) in the short term (left panel) and long term (right panel). Corresponding quantitation graphs show short term (left) and long term (right) (b) Comparison of number of bone marrow number of IgG1+ ASCs per million cells in the WT and CD40LΔ5 mice. Significance was assessed by student's unpaired t-test where *$p < 0.05$; **, $p < 0.005$; and ***, $p < 0.0005$ was considered significant. Individual mice shown with the mean and SEM. NS not significant.

To understand whether the relative percentage of total plasma cells are affected by the mRNA stability pathway, we immunized the mice using SRBCs, a poly-antigenic T dependent immunogen that would generate a much more magnified immune response. Eight days post SRBC challenge, we assessed the phenotype in the B220 positive splenocytes with the plasma cell marker CD138. There was a significant reduction in the percentage of CD138+ cells in the CD40LΔ5 spleen in response to SRBC immunization (**Figure II-5**a).

Additionally, we analyzed intracellular IgG1 and IgM within the CD138+ population. Interestingly, although the IgG1+CD138+ population was significantly lowered in the CD40LΔ5, a significant increase in the percentage of IgM+CD138+ plasma cells was observed in the CD40LΔ5 mice (**Figure II-5**b). To further understand why the CD40LΔ5 had increased IgM isotype distribution, we analyzed the CD93 (long lived plasma cell marker) positive populations of both IgG1+CD138+ and IgM+, CD138+ plasma cells. The CD93+IgM+CD138+ and the CD93+IgG1+CD138+ populations were significantly higher in the wild type compared to the CD40LΔ5 (**Figure II-5**c), indicating that IgM+ plasma cells in the CD40LΔ5 mice are relatively short lived.

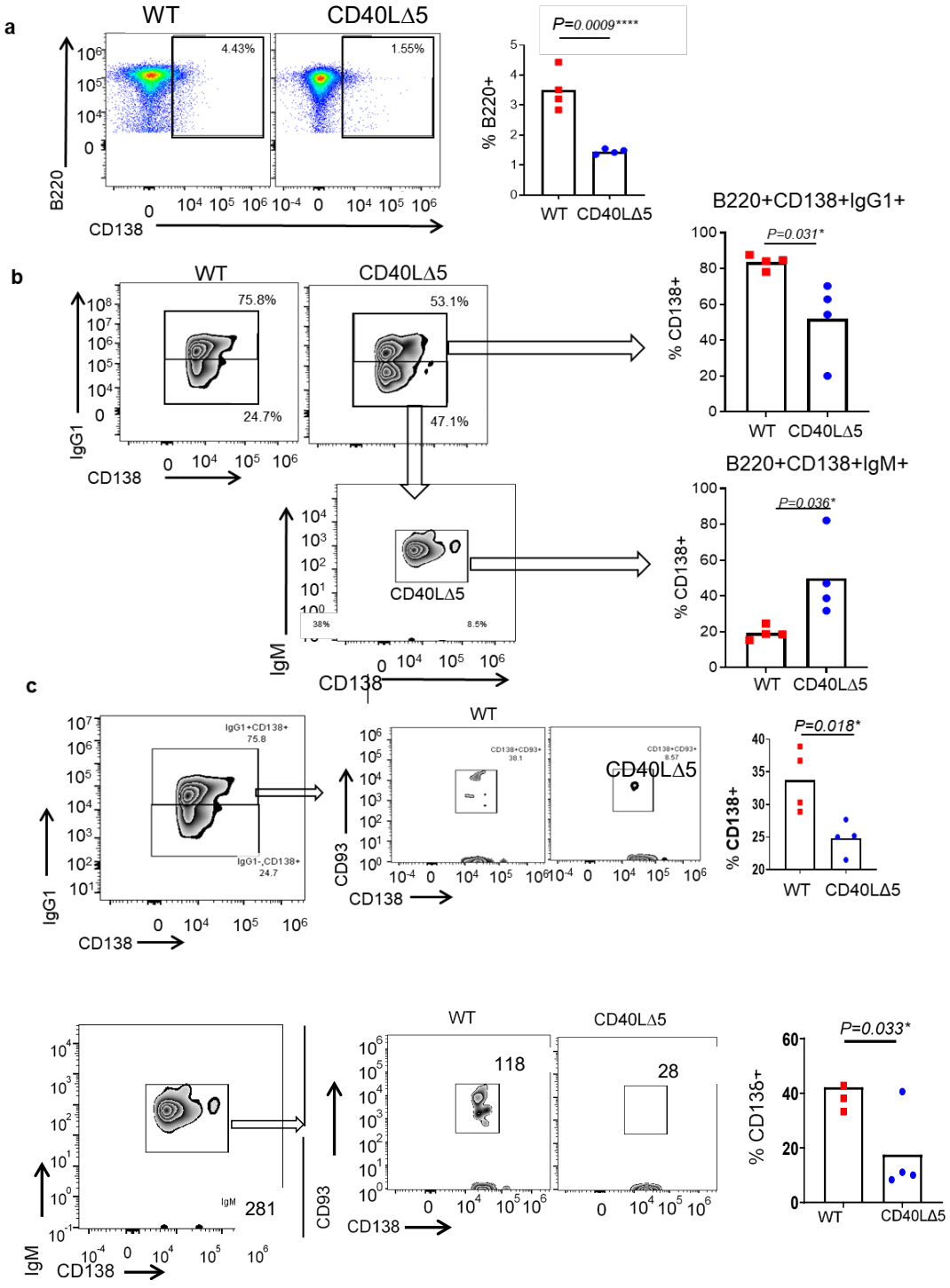
a
WT
CD40LΔ5
4.43%
1.55%
B220
CD138
P=0.0009****
% B220+
WT CD40LΔ5
b
WT
CD40LΔ5
75.8%
24.7%
53.1%
47.1%
IgG1
CD138
B220+CD138+IgG1+
P=0.031*
% CD138+
WT CD40LΔ5
CD40LΔ5
IgM
CD138
B220+CD138+IgM+
P=0.036*
% CD138+
WT CD40LΔ5
c
IgG1+CD138+
75.8
IgG1-,CD138+
24.7
IgG1
CD138
WT
CD40LΔ5
CD93
CD138
P=0.018*
% CD138+
WT CD40LΔ5
IgM
281
IgM
CD138
WT
CD40LΔ5
118
28
CD93
CD138
P=0.033*
% CD136+
WT CD40LΔ5

Figure II-5 Decreased number of plasma cells observed in the CD40LΔ5 spleens. WT and CD40LΔ5 spleens, 8 days post SRBC immunization were collected and evaluated for CD138+ B220+ plasma cells. (a) Representative dot plot showing CD138+ plasma B cells in splenocytes from WT and CD40LΔ5 mice (left), and quantitated percentages of B220+/low cells expressing CD138, WT (red) CD40LΔ5 (blue). (b) Representative dot plot showing CD138+IgG1+ and CD138+IgM+ B cells in the WT and CD40LΔ5 mice (left) and corresponding quantitated percentages (right). (c) Representative density plots showing CD93+ IgG1+CD138+(top right) and CD93+ IgG1+CD138+ B cells in WT and CD40LΔ5 mice (bottom left) Consolidated average of CD93+ long lived plasma cells of IgG1+(top right) and IgM+ (bottom right) isotypes. Graphs represent each individual mouse as blue dots (CD40LΔ5) or red square (WT) and average as the top of boxed bars. Significance estimated as $p>0.05$ by students unpaired t test.

To understand the impact of the activation induced mRNA stability pathway on the migration of plasma cells to the bone marrow we compared the relative distribution of plasma cells in the bone marrow of WT and CD40LΔ5 mice. Bone marrows were collected from mice post immunization with SRBCs and stained for plasma cell marker CD138 and long-lived plasma cell marker CD93. The percentage of CD138+B220+ plasma cells was decreased significantly in the CD40LΔ5 mice (**Figure II-6**a). On further evaluation with the long-lived plasma marker CD93, we also saw that the percentage of CD93+CD138+B220+ plasma cells were significantly reduced in the CD40LΔ5 bone marrows when compared to the wild type (**Figure II-6**b).

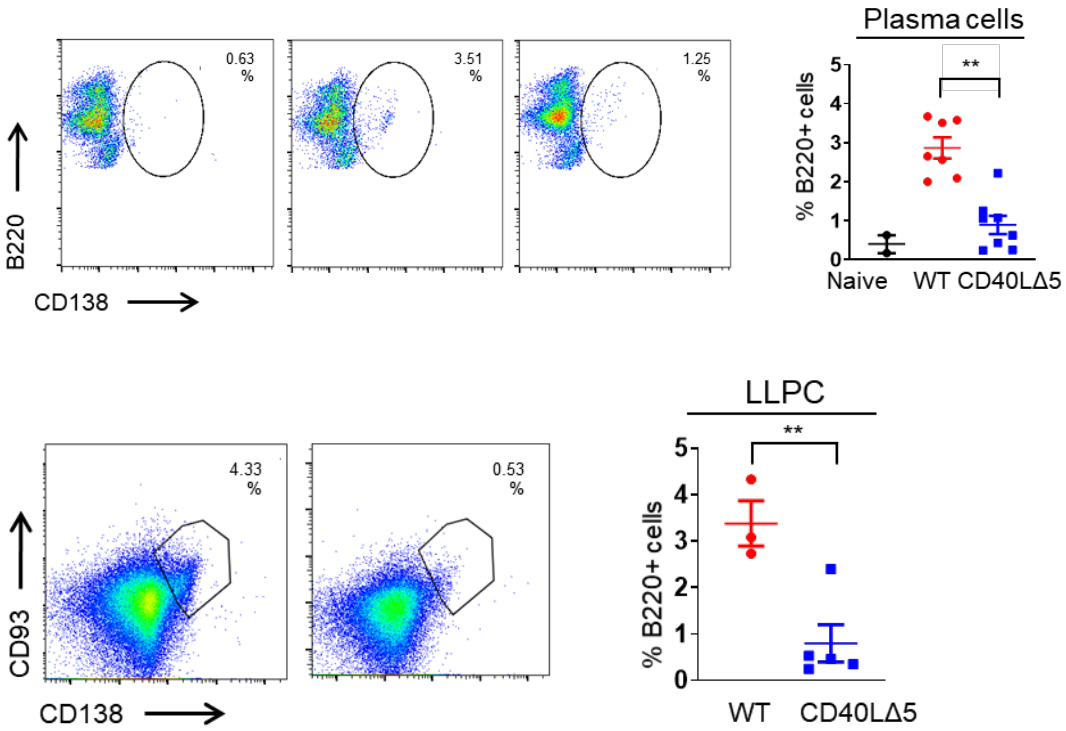

Figure II-6 Decreased number of plasma cells observed in the CD40LΔ5 bone marrow.
WT and CD40LΔ5 bone marrow aspirate cells were collected 8 days post SRBC immunization and evaluated for CD138+ B220+ plasma cells. (a) Percentage of plasma B cells in the bone marrows of WT and CD40LΔ5 mice. (b) Percentage of CD93+ CD138+ B cells shown in the WT and Δ5 deleted mice. Significance was assessed by student's unpaired t-test where *$p < 0.05$; **, $p < 0.005$; and ***, $p < 0.0005$ was considered significant. Individual mice shown with the mean +/-SEM.

Size and organization but not the number of GCs is affected in the CD40LΔ5

To evaluate whether the decreased level of plasma cells was a direct impact of impaired GC formation, we assessed the GC structure and organization. Dissociated splenocytes stained with GL7 and Fas markers were used to identify GC B cells in the B220 positive population. There was a significant reduction in the percentage GL7/Fas positive cells in the spleens of the CD40LΔ5 mice (**Figure II-7**a). In striking contrast, when we looked at the Tfh cell populations, there was no significant difference in the distribution of CXCR5+ PD-1+ CD4 T cells (**Figure II-7**b). In addition to flow, immunohistochemistry was used to evaluate the GC morphology and organization. Multiple images of hematoxylin/eosin (H&E) stained, frozen 20µm sections were evaluated for GC structure. In CD40LΔ5 mice the GC structure was much less compact and irregularly shaped than the WT (**Figure II-7**c). Antibodies against GL7 (GC cells), anti-IgD (mature naïve B cells) and CD4 (T cell) were used to delineate specific regions of the GC. GCs in WT spleens were more organized with well-defined regions of GL7 and IgD. The CD40LΔ5 mice had loosely organized GCs with scattered GL7 cells within IgD positive areas (**Figure II-7**d). Although the average number of GCs per frame was not significantly different in the wild type and the CD40LΔ5 mice (**Figure II-7** e), there was a significant decrease in the area of each GC (**Figure II-7** f).

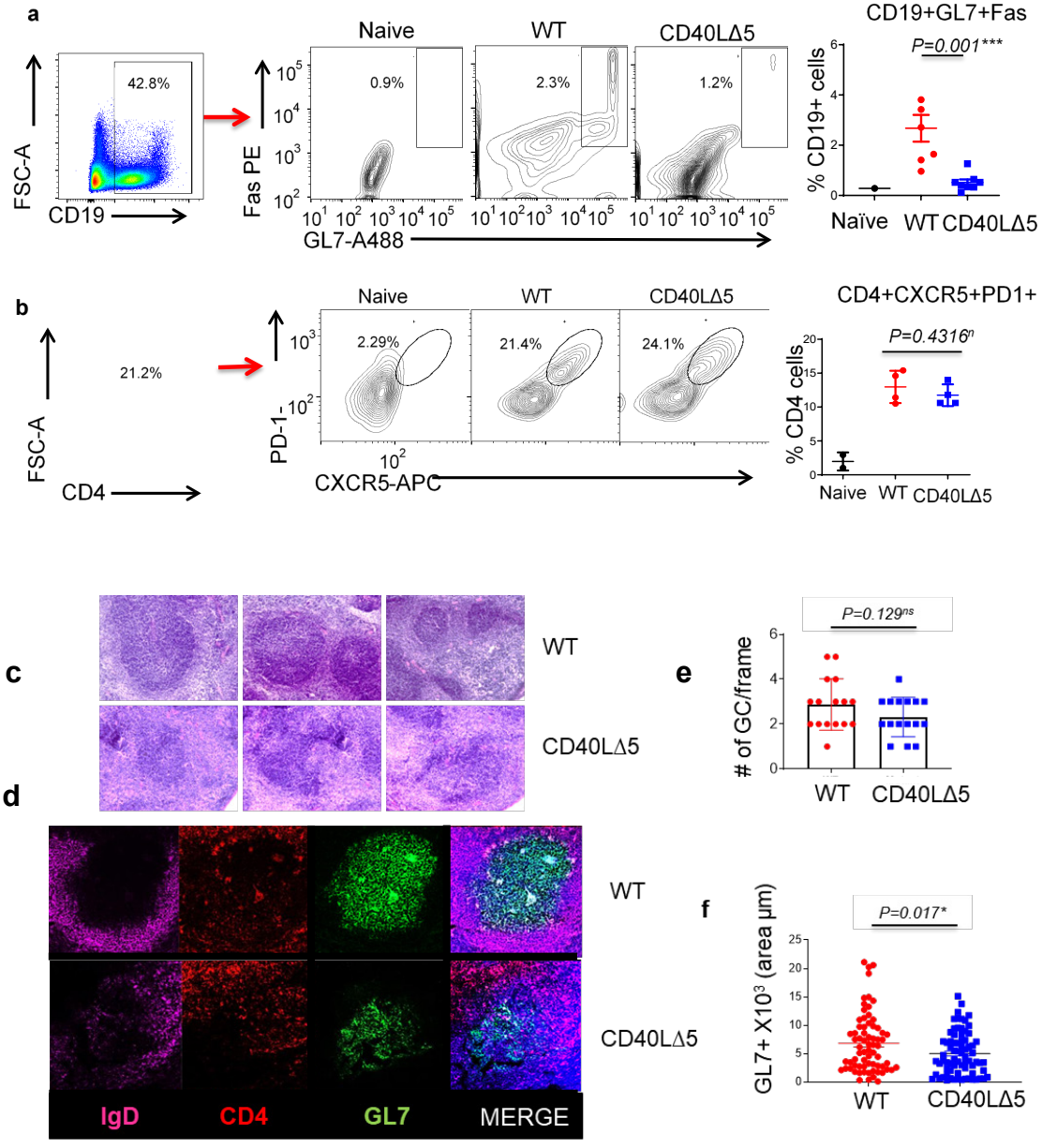
a
FSC-A
CD19
42.8%
Naive
WT
CD40LΔ5
Fas PE
GL7-A488
0.9%
2.3%
1.2%
CD19+GL7+Fas
P=0.001***
% CD19+ cells
Naïve
WT
CD40LΔ5
b
FSC-A
CD4
21.2%
PD-1
CXCR5-APC
2.29%
21.4%
24.1%
CD4+CXCR5+PD1+
P=0.4316ns
% CD4 cells
c
WT
CD40LΔ5
d
IgD
CD4
GL7
MERGE
e
P=0.129ns
# of GC/frame
f
P=0.017*
GL7+ X10³ (area µm)

Figure II-7 Decreased CD40L mRNA stability affects the population of GC B cells but not CD4 T cells.

Splenocytes were isolated from naïve and WT and CD40LΔ5 mice, 8 days post SRBC immunization and analyzed by flow cytometry. (a) Representative dot plots showing GL7+ Fas+ CD19+ cells from naïve, WT and CD40LΔ5 mice (left). Consolidated data of GL7+Fas+ CD19+ cells from 6 individual mice from each group (right) (b) Representative dot plots showing CXCR5+PD-1+ CD4 T cells from naïve, WT and CD40LΔ5 mice (left).). Consolidated data of CXCR5+PD-1+ CD4 T cells from 6 individual mice from each group (right) (c) GC structure 8 days post SRBC immunization with 20μm sections from frozen spleens stained with hematoxylin and eosin (H&E). (d) Splenic sections were stained for mature naïve B cells (IgD, magenta), T cells (CD4, red), and GC B cells (GL7, green). Images were acquired using a Nikon Eclipse E600 brightfield microscope or Zeiss LSM810 confocal microscope. (d) The GCs were identified using Olympus Studio 2 software and the number of GC per image frame calculated. The area of each individual GC was also quantitated using the same software and number of GCs (e) and the GC area (f) for WT (red) and CD40LΔ5(blue). Significance was assessed by student's unpaired t-test where *$p < 0.05$; **, $p < 0.005$; and ***, $p < 0.0005$ was considered significant. Individual mice shown with the mean +/- SEM.

Larger proportion of CD40LΔ5 GC B cells are present in the LZ

Increased percentage of DZ GC B cells is an indication of higher rate of successful T cell help [115, 123]. Therefore, GC B cells from wild type and CD40LΔ5 mice were evaluated for distribution into the LZ and DZ to understand the effect of lowered CD40L expression on the distribution of B cells into each zone. We used to markers CXCR4, a marker expressed highly on dark zone B cells and CD86 a marker used to define the light zone GC B cells, to evaluate the distribution of GC B cells into different zones. Splenocytes were evaluated 8 days post SRBC immunization for LZ ($CD19^{+}GL7^{+}CD86^{hi}CXCR4^{lo}$) and DZ ($CD19^{+}$ $GL7^{+}$ $CD86^{lo}CXCR4^{hi}$) B cell distribution by flow cytometry. The CD40LΔ5 had significantly lower percentages of DZ GC B cells compared to wild type and this corresponded to an increase in LZ B cells relative to wild type (**Figure II-8**a). Immunohistochemistry on the spleens using CXCR4 (DZ), CD21/CD35 and CD23 (LZ) revealed a similar reduction in the DZ area in the CD40LΔ5 (**Figure II-8**b).

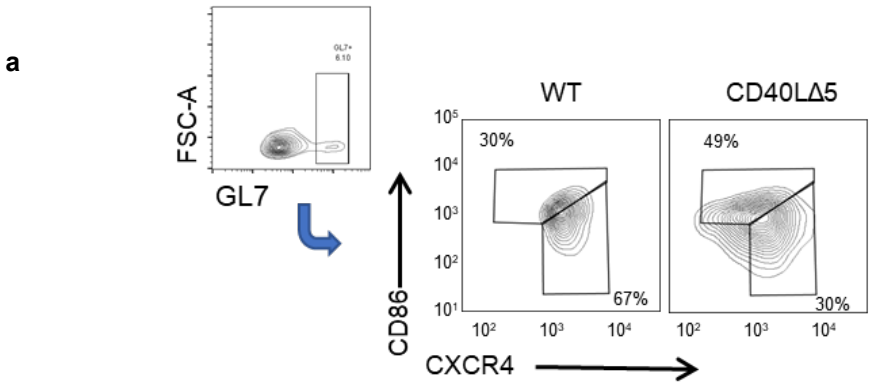
a
FSC-A
GL7
WT
CD40LΔ5
30%
67%
49%
30%
CD86
CXCR4

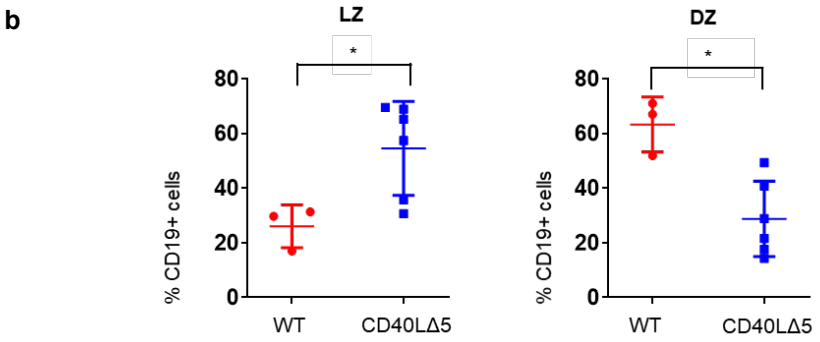
b
LZ
DZ
% CD19+ cells
WT
CD40LΔ5

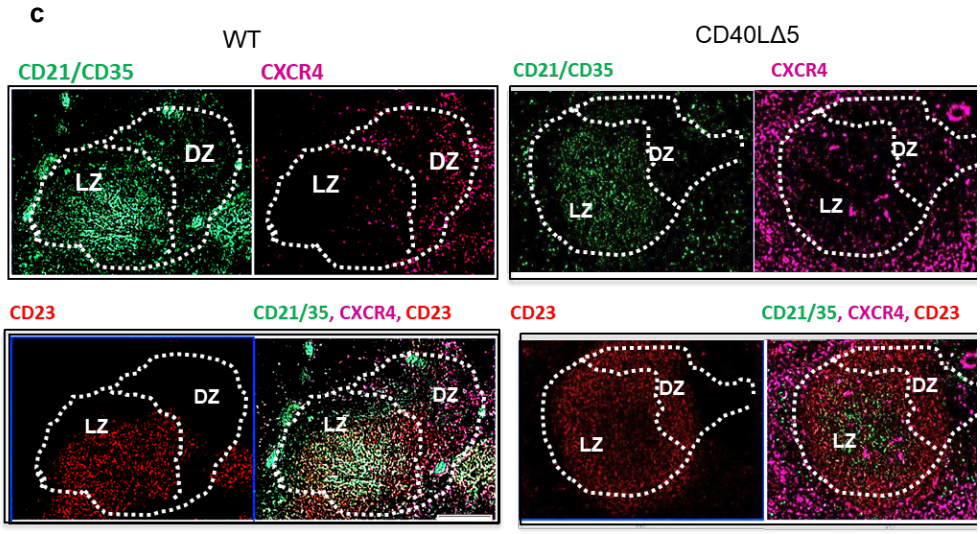
c
WT
CD40LΔ5
CD21/CD35
CXCR4
CD23
CD21/35, CXCR4, CD23
LZ
DZ

Figure II-8 LZ/DZ distribution of B cells affected by the Δ5 deletion.
WT and CD40LΔ5 mice spleens 8 days post SRBC immunization were dissociated. The percentage of CD86 ^{hi} and CXCR4 ^{hi}, GL7+ GC B cells was estimated using flow cytometry. (a)Representative contour plots show CXCR4^{hi}(DZ) and CD86 ^{hi} (LZ) populations in WT and CD40LΔ5 mice. (b). Consolidated percentages of LZ (CD86 ^{hi} GL7+, left) and DZ (CXCR4 ^{hi} GL7+, right) cell from n=3, WT and n=6, CD40LΔ5 mice. c) Representative images from 20μm sections were collected from frozen spleens from 3 wild type and 4 CD40LΔ5, fixed and stained for LZ (CD21/35, green or CD23, red) and DZ (CXCR4, magenta) distribution. Statistical significance determined as $p<0.05$ by students unpaired two tailed t-test. Each symbol represents an individual mouse and the mean and SEM shown.

Memory B cell precursors are reduced in CD40LΔ5

To understand whether the activation induced stabilization of CD40L transcript is essential to generate memory B cells we compared CD19+IgG1+, CD38+ memory precursor B cells in the WT and CD40LΔ5 mice. There was a significant reduction in the percentages of CD38+/IgG1+ memory precursors in the spleens of CD40LΔ5 mice when compared to the WT (**Figure II-9**a).

The level of the CD40/CD40L interactions determines ability of B cells to differentiate into specific memory subsets like $CD80^{hi}$ B memory cells [65]. So as to understand the impact of the Δ5 mutation on distinct memory subsets, we evaluated the memory markers PD-L2, CD80 and CD73 in IgM and IgG1 positive cells, and these markers showed marked decrease in expression in CD40LΔ5 mice relative to wild type (**Figure II-9**b,c).

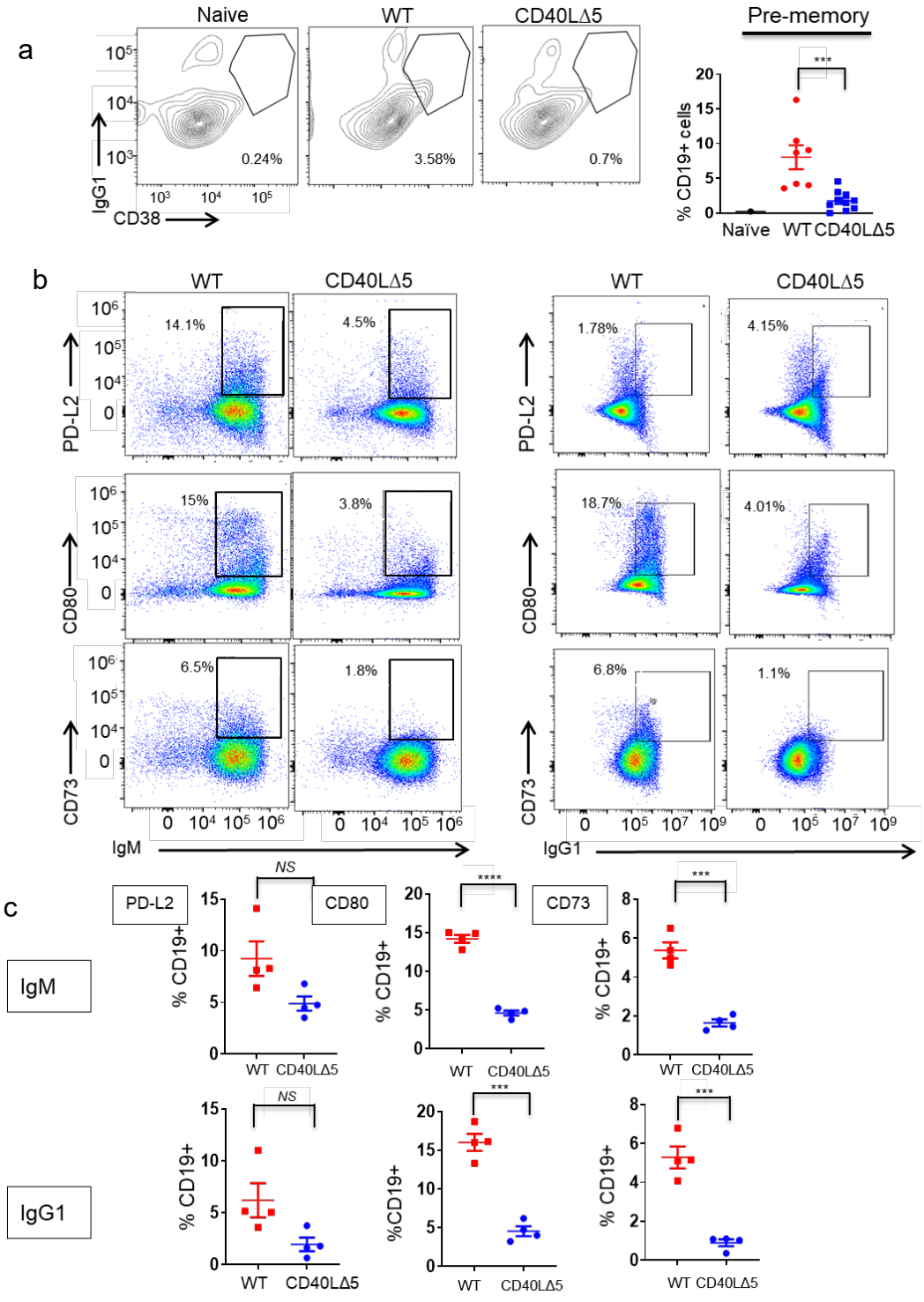
a
Naive
WT
CD40LΔ5
Pre-memory
IgG1
CD38
0.24%
3.58%
0.7%
% CD19+ cells
Naïve
WT
CD40LΔ5
b
WT
CD40LΔ5
PD-L2
CD80
CD73
IgM
IgG1
14.1%
4.5%
1.78%
4.15%
15%
3.8%
18.7%
4.01%
6.5%
1.8%
6.8%
1.1%
c
PD-L2
CD80
CD73
IgM
IgG1
% CD19+
%CD19+
NS
WT
CD40LΔ5

Figure II-9 Decreased memory B cell populations in the CD40LΔ5 mice:
WT and CD40LΔ5 mice spleens 8 days post SRBC immunization were dissociated and percentage of isotype switched CD38+ cell and memory marker subsets (PD-L2+, CD80+ and CD73+) expressing IgM and IgG1 cells was evaluated using flow cytometry. (a) CD38+IgG1+Cd19+ B cells were evaluated in WT and CD40LΔ5 mice, representative image left, quantitation of results with individual mice depicted as red dots (WT), blue squares (CD40LΔ5) and black dots (naïve) right. (b) Representative dot plots of PD-L2 (top), CD80 (middle) and CD73 (bottom) with IgM left and IgG1 right. (c) Quantitation of population distribution of IgM (top) and IgG1 (bottom) expressing B cells with PD-L2 (left), CD80 (middle) and CD73 (right) wild type mice depicted as red squares and CD40LΔ5 as blue dots. Significance was assessed by student's unpaired t-test where *$p < 0.05$; **, $p < 0.005$; and ***, $p < 0.0005$ was considered significant. Individual mice shown with the mean +/- SEM.

Proliferation pathway is impaired in B cells in the CD40LΔ5 mice

To further understand the impact of the mRNA stability pathway on B cell development and differentiation we conducted RNAseq analysis on CD19+ B cells. The evaluation of significant differentially expressed genes showed that several of the genes that were downregulated in the CD40LΔ5 mice were associated with proliferation (**Figure II-10**a). Further evaluation of pathways negatively impacted by the decreased mRNA stability of CD40L included the cell cycle and mitosis pathways (**Figure II-10**b). Of the genes that were upregulated in the CD40LΔ5 some were linked to apoptosis (**Figure II-10**a). We did not however see a significant upregulation of apoptosis pathways by pathway analysis. Specific genes that were downregulated in the CD40LΔ5 included Bcl6 (GC), CCL22 (T cell attracting cytokine) and CD93 (long lived plasma cells). Innate immunity associated genes as C4a, Lair1, Ifi27 and Irf7 were upregulated in the CD40LΔ5 mice. Il9r, a receptor implicated in memory B cells was also interestingly upregulated in the CD40LΔ5 mice (**Figure II-10**c).

a

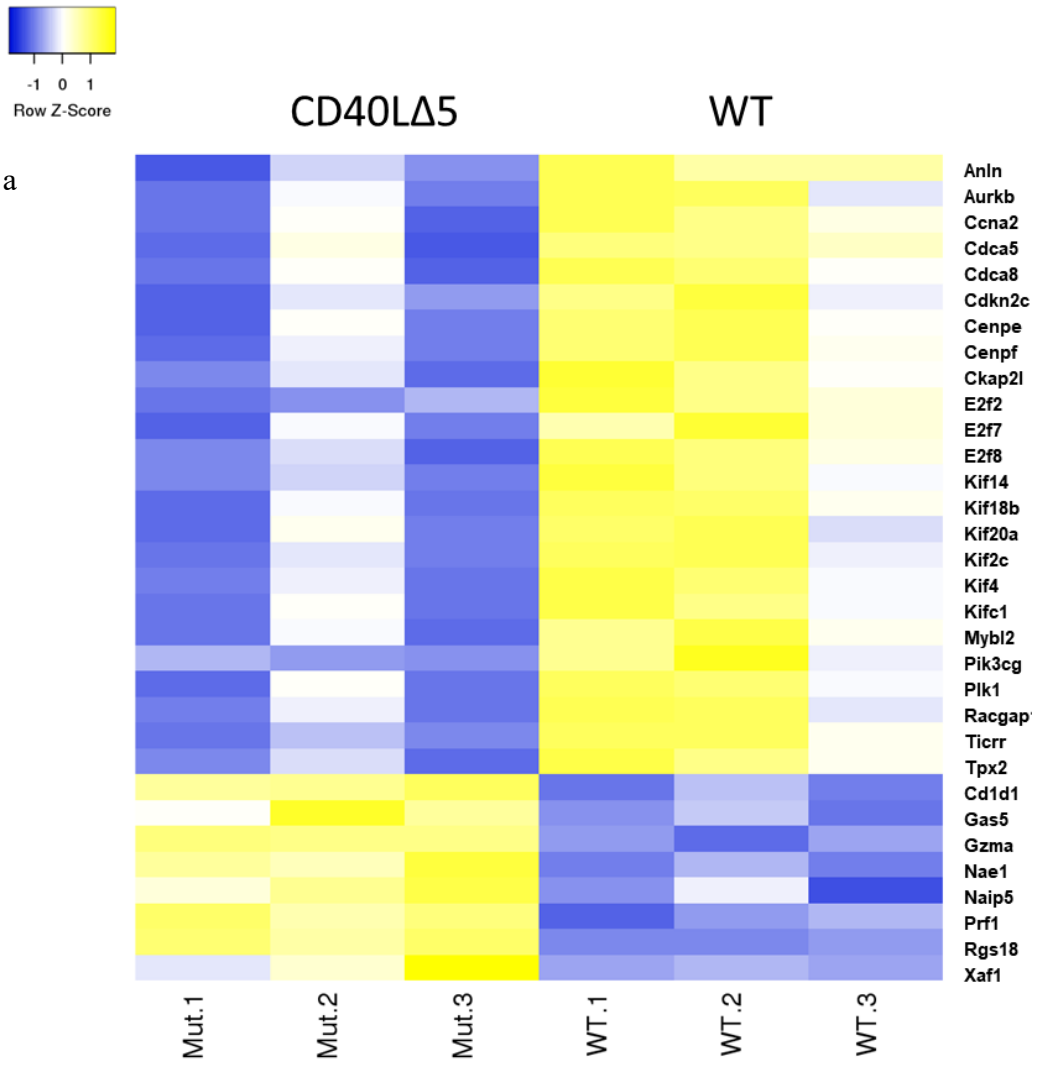
-1 0 1
Row Z-Score
CD40LΔ5
WT
Anln
Aurkb
Ccna2
Cdca5
Cdca8
Cdkn2c
Cenpe
Cenpf
Ckap2l
E2f2
E2f7
E2f8
Kif14
Kif18b
Kif20a
Kif2c
Kif4
Kifc1
Mybl2
Pik3cg
Plk1
Racgap
Ticrr
Tpx2
Cd1d1
Gas5
Gzma
Nae1
Naip5
Prf1
Rgs18
Xaf1
Mut.1
Mut.2
Mut.3
WT.1
WT.2
WT.3

b

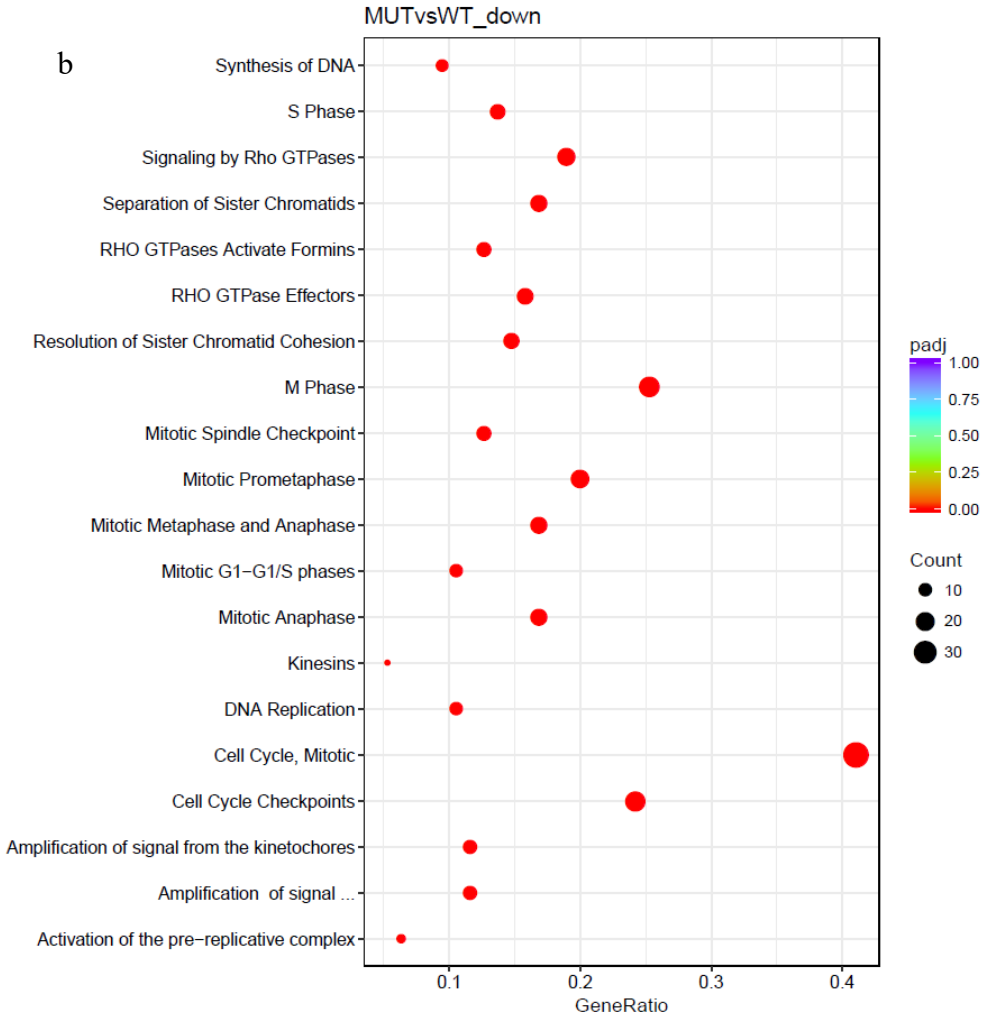
MUTvsWT_down
Synthesis of DNA
S Phase
Signaling by Rho GTPases
Separation of Sister Chromatids
RHO GTPases Activate Formins
RHO GTPase Effectors
Resolution of Sister Chromatid Cohesion
M Phase
Mitotic Spindle Checkpoint
Mitotic Prometaphase
Mitotic Metaphase and Anaphase
Mitotic G1−G1/S phases
Mitotic Anaphase
Kinesins
DNA Replication
Cell Cycle, Mitotic
Cell Cycle Checkpoints
Amplification of signal from the kinetochores
Amplification of signal ...
Activation of the pre−replicative complex
0.1
0.2
0.3
0.4
GeneRatio
padj
1.00
0.75
0.50
0.25
0.00
Count
10
20
30

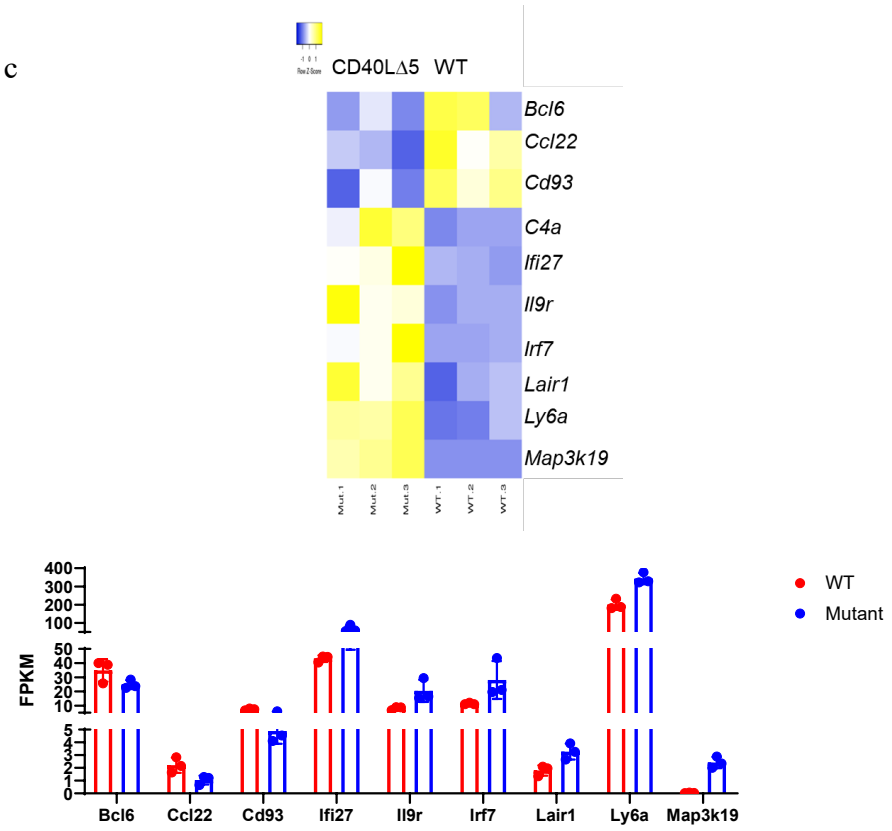

Figure II-10 mRNA stability pathway–deficient GC B cells fail to up-regulate genes involved in mitosis, cell cycle and proliferation.
RNA was isolated CD19+ B cells using Mojosort positive isolation kit and DNA library generated using NEB Next Ultra RNA Library Prep Kit for Illumina, sequenced on a HiSeq 1500 sequencer (Illumina) in a 49-bp single-end read mode and the raw data processed with CASAVA 1.8.2 (Illumina). B cell fractions were isolated 3 mice per genotype were evaluated. (a) Heat map of differentially expressed genes with at least 30% upregulation or down regulation shown color coded for z-score (expression difference/standard deviation) relative to the mean with dark blue showing lower levels and bright yellow indicating the high scores. (b) GO pathway analysis showing significantly ($p<0.05$) downregulated pathways with dot size correlating number of genes in the pathway that are down regulated. (c) Differentially expressed genes shown with corresponding degree of change from dark blue lowest levels to bright yellow, highest levels.

Decreased proliferation and increased apoptosis in GC B cells

Since we evaluated the total B cells by RNA seq we wanted to confirm that the changes in proliferation and apoptosis could be linked to changes in the GC B cells. To evaluate whether GC B cell proliferation and apoptosis are affected by the Δ5 mutation, we looked at proliferation and apoptosis markers by flow cytometry. Total splenocytes were collected 8 days post immunization with SRBCs and evaluated for surface B220 and GL7 and intracellular Ki67 (proliferation) and phospho-histone H3 (mitotic marker). The percentage of cells positive for Ki67 was significantly lower in the CD40LΔ5 when compared to the WT. Similarly, phospho-histone H3, a marker for mitotic potential was significantly reduced in the CD40LΔ5 as well (**Figure II-11**a,b). To understand if the spatial distribution of proliferating GC B cells is affected by the Δ5 mutation, splenic tissue sections from WT and CD40LΔ5 mice were stained for mature naïve B cells (IgD+), GC B cells (GL7+) and proliferating cells (Ki67+) and fluorescent images analyzed. There were lower number of GL7, Ki67 double positive foci in the CD40LΔ5 when compared to the WT (**Figure II-11**c).

We evaluated intracellular activated Caspase-3 and cleaved PARP in GC B cells to understand whether the CD40LΔ5 mutation could result in more GC B cells undergoing apoptosis. We observed significantly higher levels of activated Caspase-3 and cleaved PARP in the GCs of CD40LΔ5 mice (**Figure II-11**d).

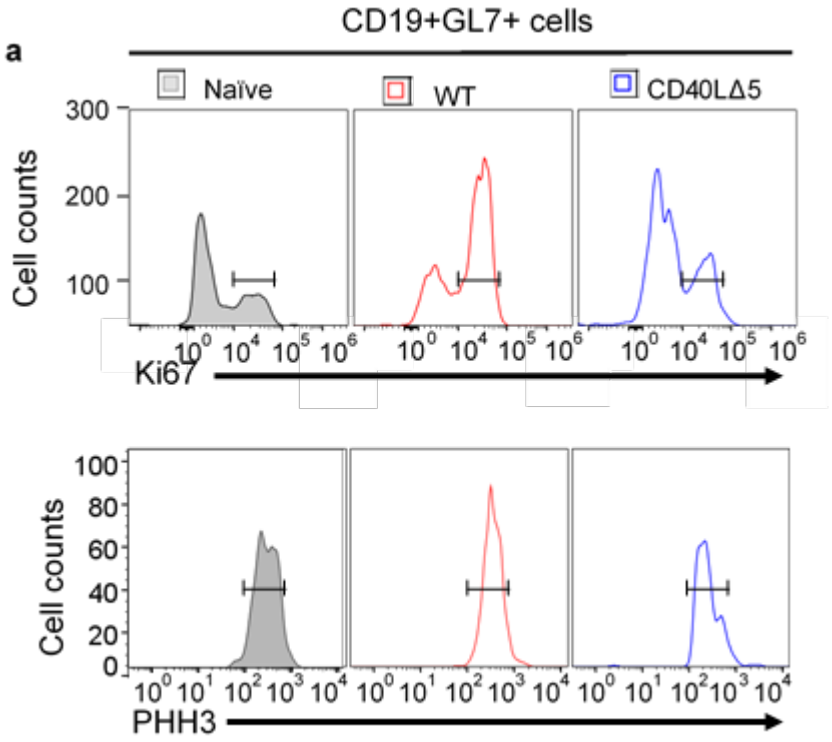
a
CD19+GL7+ cells
Naïve
WT
CD40LΔ5
Cell counts
300
200
100
Ki67
Cell counts
100
80
60
40
20
0
PHH3

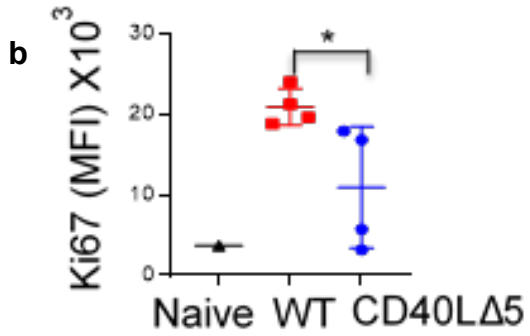
b
Ki67 (MFI) X10^3
30
20
10
0
*
Naive WT CD40LΔ5

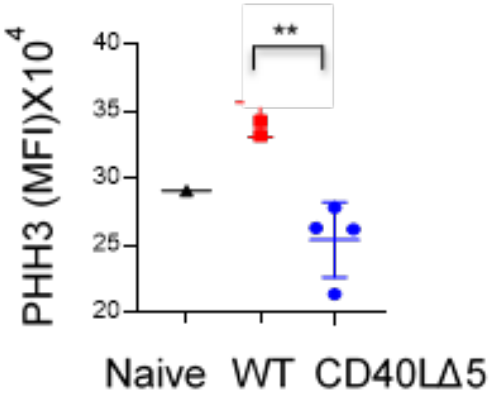
PHH3 (MFI)X10^4
40
35
30
25
20
**
Naive WT CD40LΔ5

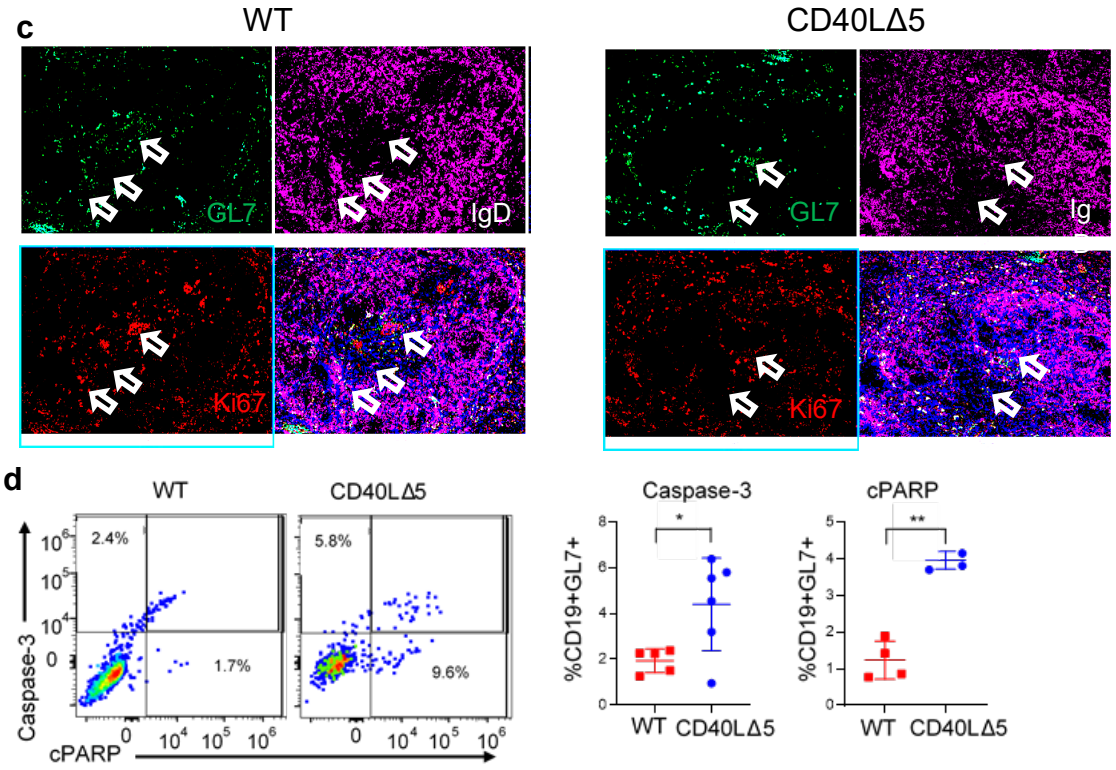

Figure II-11 Decreased proliferation and increased apoptosis in CD40LΔ5 GL7 B cells.

(a) Dissociated splenocytes from WT and CD40LΔ5 mice 8 days post SRBC immunization. were subject to flow-cytometric analysis gated on GL7+ B cells for expression of Ki67 (top) and phospho-histone H3 (PHH3) (bottom). (b) Mean fluorescence intensity data form (a) shown. (c) Splenic tissue sections from the same mice were stained for mature naïve B cells (IgD+, magenta) to demarcate GCs, GC B cells (GL7+, green) and proliferating cells (Ki67, red) and imaged using a Nikon Eclipse E600 fluorescence microscope with a XM-20 digital color camera. Areas of overlap of Ki67 and GL7 subset are marked by white arrows. (d) Intracellular activated Caspase-3 and cleaved PARP in GL7+B220+ splenic cells by flow cytometry. Representative dot plots (left panel) with WT (left) and CD40LΔ5 (right). Quantitation of n=2 experiments with WT (red) and CD40LΔ5 (blue). Significance was assessed by student's unpaired t-test where *$p < 0.05$; **, $p < 0.005$; and ***, $p < 0.0005$ were considered significant. Individual mice shown with the mean +/- SEM.

Discussion:

CD40/CD40L interaction is quintessential for the development of a robust humoral immune response. The role of CD40L in the T dependent immune response has been studied using the CD40L knockout mice as well as blocking antibodies to CD40L [85, 86, 135]. Abolishing CD40L precludes the development of germinal center in mice leaving little room for evaluation of the multitude of functional processes within the GC. The CD40L deficient model has been able to conclusively show that the absence of CD40L drastically affects affinity maturation, class switching and the memory response. But it fails to appreciate the effect of dynamic changes in surface CD40L in the context of a T dependent immune response. CD40L is modulated during different timepoints of the immune response by multiple mechanisms including transcriptional and post transcriptional regulation [21-24]. In addition, CD40L binding to CD40 upregulates ICOSL, CD80 and CD86 on GC B cells, followed by a feed forward induction of additional CD40L expression on T_{fh} cells [89]. Our over-arching goal was to understand how activation dependent kinetics of CD40L expression generate an adaptable and effective humoral response. Previous data from our lab has shown that the activation-induced regulation of CD40L by a novel post-transcriptional mRNA stability pathway is one of the mechanisms by which the expression of CD40L is regulated during the immune response. Here, we demonstrate that the expression level of CD40L, as modulated by the mRNA stability pathway, plays a central role in the progression of a T dependent immune response.

It has been well established that CD40 or CD40L defective patients and mouse models have significant decreases in serum IgA and IgG predisposing them to bacterial

infections [85, 136, 137]. However, the threshold of CD40L expression required to significantly impact antibody production is not well understood. The CD40LΔ5 model expressing lower levels of CD40L at a more advanced stage of activation presents significant decreases in all expressed IgG isotypes with the IgM titers reduced only in the secondary response. This suggests that a threshold level of CD40L is required to facilitate an effective antibody response and the CD40L expression in the CD40LΔ5 mice is below this threshold.

CD40L deficiency is associated with decreases in two critical factors, AID and uracil-DNA glycosylase 2 (UNG-2), that are essential for SHM and subsequent affinity maturation [137]. CD40/CD40L interaction is critical for selection of high affinity B cell clones. The high affinity clones have greater ability to present antigen-derived peptides in the context of MHC class II and during the TCR engagement it triggers downstream signaling which increases the surface expression of CD40L on T_{fh} cells [41, 138]. We discovered that limiting CD40L signaling resulted in reduced affinity maturation in the secondary response but not in the primary response. This suggests that the threshold of CD40L expression in the CD40LΔ5 does not entirely preclude SHM. However, the CD40LΔ5 has lower level of high affinity clones as the GC reaction progresses. We conclude that the decreased threshold of CD40L in the CD40LΔ5 mice is insufficient for the B cells to acquire the optimal permissive signals to undergo multiple rounds of SHM. In addition, the fact that proliferation of GC B cells is drastically affected, could be a contributing factor to the decrease in high affinity clones in the CD40LΔ5 model. Since our model does not abolish the expression of CD40L, we find that under conditions of limited CD40L expression, SHM still occurs albeit at a lower rate in the CD40LΔ5 mice.

Recent GC models suggest that affinity maturation, in vivo, is a consequence of repeated cycling of GC B cells between the center for SHM and proliferation, the DZ and antigen dependent affinity selection in the LZ [49, 58, 115, 123]. GC B cells dynamically migrate between the light (LZ) and dark zone (DZ) as the development of the germinal center progresses [58, 115, 123]. CD40L-dependent selection in the LZ guides the GC B cells to either recycle back to the DZ for additional rounds of mutation or leave the GC as memory or plasma cells [139, 140]. Our data suggest that in the CD40LΔ5 mice, weakened CD40L signaling during the progression of the germinal center reaction prevents the GC B cells that migrate into the LZ from receiving effective survival signals from the T_{fh}. These signals allow the GC B cells return to the DZ for further rounds of SHM or exit the GC as memory or high affinity plasma cells. In the absence of the necessary threshold of helper signals, these B cells either remain in the LZ or undergo apoptosis. When compared to wild type controls, we observed a significantly higher number of GC B cells in CD40LΔ5 expressed high levels of CXCR4, and this is indicative of their localization in the LZ. This demonstrates that the PTBP1-binding and subsequent stabilization of the CD40L mRNA is essential for maintaining a level of CD40L that is required for the functional distribution of the GC B cells into the DZ and LZ.

The role of CD40 signaling in cell proliferation and survival has been extensively studied. The CD40/CD40L interaction provides the signal for G1 stage GC B cells to enter the S phase [141]. Additionally, it has been shown that the combination of BCR and CD40 signals induce c-Myc expression and generate p-S6, both of which are required for reentry into the cell cycle [142, 143]. To understand whether the threshold levels of

CD40L expression in our model was sufficient to induce changes in the cell cycle, we assessed the gene expression profile for B cells in the CD40LΔ5. Evaluation of differentially expressed genes in the CD40LΔ5 B cells by RNAseq, showed down regulation of multiple genes associated with mitosis and cell cycle. We found Ccna2, a protein that controls both the G1/S and the G2/M transition phases of the cell cycle and E2f2, a transcription factor that functions in the control of cell-cycle progression from G1 to S phase to be significantly downregulated in the Δ5 mice. In addition, Pik3cγ which functions in activating signaling cascades involved in cell growth, survival and proliferation, as well as Mybl2, a transcription factor involved in the regulation of cell survival, proliferation, and differentiation were also downregulated in the CD40LΔ5 B cells. Multiple kinesin family members, Kif2c, Kif4, Kif14, Kif 18b, Kif 20a, which regulate cell growth through modulation of cell cycle progression and cytokinesis also had decreased expression. Finally, Aurkb, a key regulator of mitosis was found to be significantly reduced in the Δ5 mice. Since the RNAseq analysis was carried out with CD19+ B cells, we wanted to confirm that our results translate to the GC B cells using flow cytometry. Decreased Ki67 and phospho-histone H3, on gated GL7+ GC B cells in CD40LΔ5 mice gives us further confidence that the mRNA stability pathway has a direct effect on proliferation of GC B cells. Thus, we find that a major outcome of limiting CD40L is that proliferation is dramatically reduced as revealed by the specific downregulation of cell cycle and mitotic pathways.

It has been well documented that diminished T_{fh} help results in increased number of GC B cells undergoing apoptosis [44, 50, 78, 144]. Upregulation of expression of pro-apoptotic markers, Caspase-3 and cPARP in the CD40LΔ5 mice, is an indication of the

progression of GC B cells towards apoptosis. The CD40LΔ5 mice have significantly higher levels of these apoptotic markers. Thus, our data supports a model in which reduced CD40L expression leads to decreased GC B cell proliferation and increased apoptosis. We also observed significantly lower levels of GL7+ GC B cells and redistribution of a larger percentage of GC B cells into the LZ. Both these results can be explained by reduced proliferation and the fact that proliferation occurs in the DZ in the GC.

Evaluation of the GC structure and distribution in the CD40LΔ5 mice revealed reduced sized and disorganized GCs compared to wild type. However, the number and therefore the initiation of GCs, remained unchanged. This led us to conclude that unlike the CD40L knock-out mouse where GCs are not formed, GC seeding is not affected by the activation induced pathway of CD40L expression. CD40L signaling induces the expression of the transcriptional repressor Bcl-6 which in turn inhibits expression of Blimp-1 (B lymphocyte-induced maturation protein 1), a transcription factor that regulates plasma cell differentiation in the centrocyte [145]. In the absence of CD40/CD40L signaling more centrocytes are directed to become a low affinity plasma cells and this in turn results in decreased number GC B cells and has been linked to disorganized GC architecture [146]. Notably, we found that the percentage of GL7+Fas+ GC B cells were significantly reduced in the CD40LΔ5. Moreover, reduced proliferation of GC B cells and disruption the GCs has been associated with the depletion of Foxo1 transcriptional regulator of CXCR4 which in turn is essential for dark zone localization [147]. Thus, the disorganized GC architecture in the CD40LΔ5 could be a direct consequence of the reduced proliferation. The decreased number of GC B cells is

plausibly a consequence of GC B cells not receiving enough T_{fh} help to return to the DZ to continue proliferation and subsequently leading to increased apoptosis in the LZ. We did not observe a significant decrease in the percentage of T_{fh} cells, suggesting that the impact on the humoral response is not an outcome of reduced availability of T_{fh}.

The developmental fate of the GC centrocyte is tightly linked to the strength of the CD40/CD40L interaction. Enhanced CD40L signaling in vivo has been shown to induce the differentiation of GC B cells into PCs [148]. Also, long -lived ASCs are formed later during the progression of the immune response compared to memory B cells [90, 102]. If the GC development is disrupted, GC B proliferation is diminished, and isotype switched, high affinity plasma cell numbers are reduced. We discovered that reducing CD40L expression at later stages of the GC reaction significantly lowers the percentage of total B220+CD138+IgG1+ plasma cells with a corresponding increase in the total B220+CD138+IgM+ cells. This is consistent with the fact that 1) extra-follicular IgM plasma cells are primarily generated early in the immune response before the GC stage and undergo isotype switching at later times during the response and 2) the CD40LΔ5 mice express WT levels of CD40L during the early stages of the immune response. However, both long-lived plasma cell populations (B220+IgM+CD138+CD93+ and B220+IgG1+CD138+CD93+) were reduced in the CD40LΔ5 mice when compared to the wild type demonstrating the requirement for optimal levels of CD40L in forming a long-lived plasma cell population.

It is known that the strength of the CD40/CD40L interactions determines the ability of B cells to differentiate into specific memory subsets like $CD80^{hi}$ B memory cells [65]. In one case, prolonged Tfh–B cell interactions with sufficient CD40L

expression facilitated differentiation into GC centroblasts, whereas weak transient T_{fh}-B cell interactions lead to development of memory B cells [59]. However, another report showed that strong CD40/CD40L signaling on B cells leads to the development of $CD80^{hi}$ B memory cells in the primary immune response [65]. Additionally, it has been shown that disrupted GC development has been associated with poor B cell memory responses [146]. Therefore, this question whether decreased CD40L impairs memory is still highly controversial and the threshold level of CD40L signal required for different differentiation outcomes is not clear. Our findings suggest that although reducing CD40/CD40L interactions may predispose the mice towards increased memory B cell production, the fact that the GC structure and CD40L expression are compromised in the CD40LΔ5 mouse is instrumental in memory B cell differentiation being significantly reduced.

Based on the entirety of our data we propose the following model: 1) Early Stage -During early time points after antigen exposure, CD40L expression in the CD40LΔ5 is similar to that of the wild type and the B cells seed germinal centers after initial effective interactions with T cells. 2) Later Stages Post GC initiation the GC B cells proliferate in the DZ and then transit into the LZ to receive survival signals from the T_{fh}. Weaker CD40L expression at this stage accentuates the decrease of CD40L expression by hampering feed-forward pathways. The B cell clones, receiving insufficient CD40 signaling, would either proceed to become a low affinity memory or plasma cell or undergo apoptosis. Repeated cycles of GC B cells between the DZ and LZ results in lower SHM, CSR, long-lived plasma and memory cells and as a consequence reduced class switched high affinity antibody titers (**Figure II-12**).

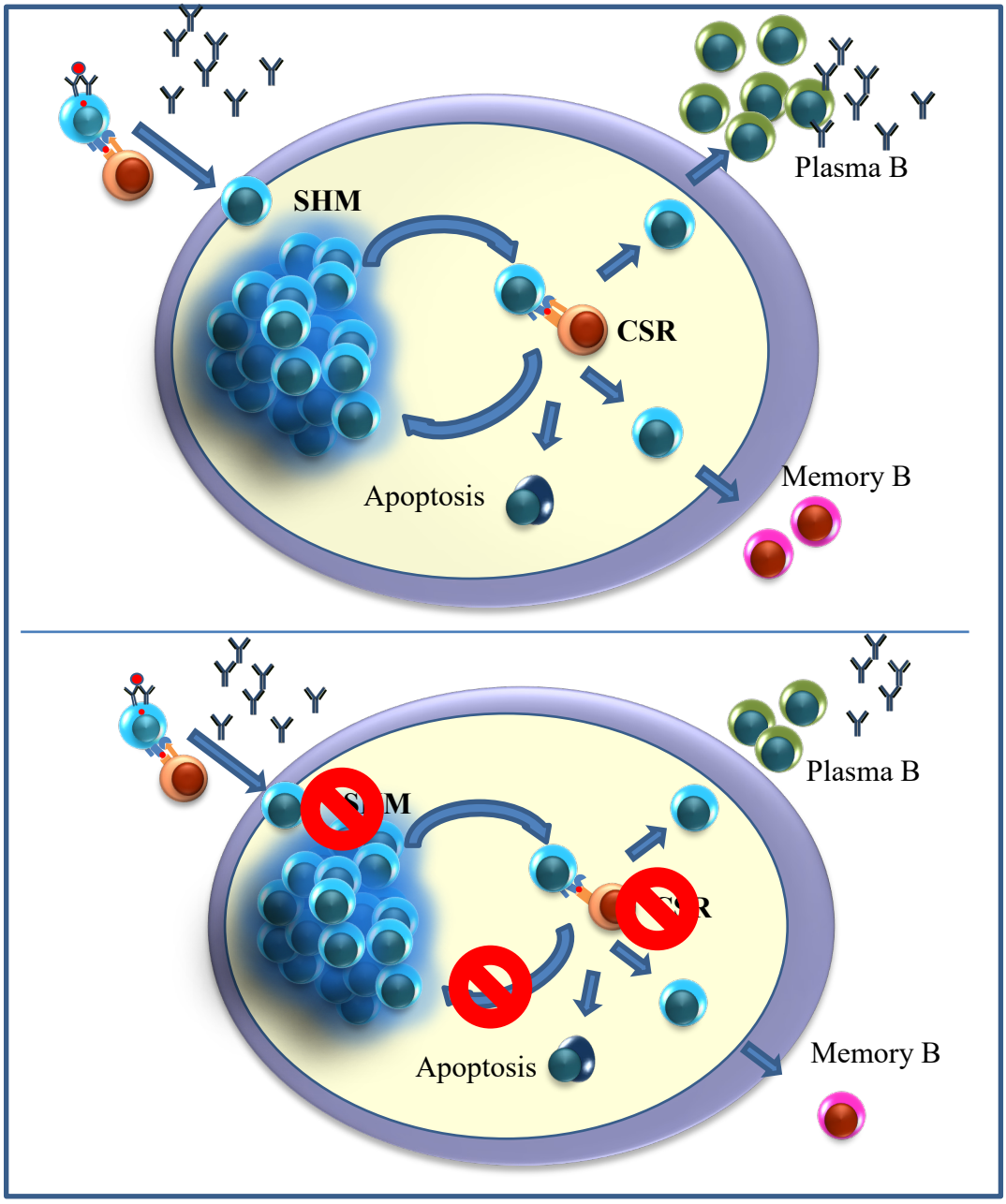

Figure II-12 Working model for the effect of PTB mediated mRNA stability

WT mice: early stage B cell-T cell interaction followed by seeding of germinal centers and subsequent proliferation, SHM, CSR and memory and high affinity plasma differentiation (top). CD40LΔ5 mice: early stage B cell-T cell interaction followed by seeding of germinal centers but reduced proliferation, SHM, CSR and memory and high affinity plasma differentiation and increased apoptosis.

Conclusion:

We have developed a model to test the importance of regulated CD40L in the development of a T-dependent humoral response. This model is based on the elimination of an mRNA stability element in the 3'UTR of the CD40L mRNA that is regulated by T cell activation.

The mRNA stability mediated regulation of CD40L is activation dependent and modulates expression depending on the requirements of the system. In naïve CD4+ T cells CD40L mRNA decay is faster and prolonged activation by binding to specific B cells is needed for increased stability of the transcript [110]. As the activation progresses the mRNA stability is one of the multiple feed forward mechanisms that dynamically regulate CD40L expression.

In addition to CD40L expression, activation induced cytokines are highly regulated in the T_{fh}. It has been reported that intrinsic changes occur in T_{fh} in response to activation, with high IL-21 production to support upregulation of Bcl6 during the early GC response, followed by switching to IL-4 production and upregulation CD40L later on in the reaction [149]. Our model with activation dependent regulation of CD40L could provide insight into the effect of decreased CD40L during the IL-4 switching in the T_{fh}.

Characterization of T dependent immune responses in the context of the CD40LΔ5 mutation revealed a critical role for dynamic levels of CD40L in affinity maturation, class switching and memory responses. The molecular basis for a majority of these findings was the significant loss of capacity within the GC B cells to undergo proliferation. However, it is unclear whether reduced proliferation is the defect

underlying the complete loss of memory B cells or whether is a consequence of decreased CD40 signals that are critical for developmental fate decisions.

Understanding how the immune system fine tunes a T-dependent response to adapt to a wide range of foreign antigens and pathogens is essential to treating immune diseases. This pathway of regulated CD40L expression may be useful in the future development of therapeutics to treat autoimmune disease. For example, the use of an antibody targeting CD40L to disrupt the CD40/CD40L engagement and subsequently treat autoimmune disease was unsuccessful due to platelet aggregation from CD40L expression and Fc receptor activity [150]. To overcome Fc mediated toxicity from the use of an antibody, a scaffold protein, VIB4920, which binds and blocks human CD40L, was developed. VIB4920 inhibits B cell activation but does not induce platelet aggregation and showed reduced rheumatoid arthritis in patients in clinical trials with no thrombotic side effects [151]. Unlike either a CD40L targeting antibody or protein, modulating the mRNA stability in response to activation does not have the potential for Fc activity or binding to undesired targets and toxicity. Thus, our model provides a potential targeting opportunity where we can use sequence specific oligos targeting the stability element, to block the binding of the PTBP1 complex to the CD40L 3'UTR reducing the CD40L expression only during the inflammatory phase. Since we are not targeting the CD40L in the absence of inflammation, this in turn could circumvent the side effects of blocking CD40L completely while alleviating the autoimmune response.

In conclusion, the CD40LΔ5 provides a unique and novel mouse model for studying the importance of regulated CD40L expression in both normal and pathogenic

immune responses. Further studies are warranted to understand the exact stages of the GC reaction which are impacted by this pathway.

Antigen	Fluor	Catalog #	Source
CD19	BV570	115535	BioLegend
IgM	BV510	406531	BioLegend
IgG1	BV650	406629	BioLegend
IgG2b	PE	406708	BioLegend
CD138	BV711	142519	BioLegend
CD93	PerCp-Cy5	136511	BioLegend
Blimp-1	Alexa 647	150003	BioLegend
CD86	APC-Fire750	105045	BioLegend
CXCR4	BV421	146511	BioLegend
CD38	Pacific Blue	102719	BioLegend
Fas	BV605	152612	BioLegend
CD73	A700	127229	Biolegend
CD80	PE/Cy7	104733	Biolegend
PD-L2	PE-Dazzle	107215	Biolegend
B220	APC	103211	Biolegend
GL7	Alexa 488	144611	Biolegend
IL-9R	Purified	MAB2134-SP	R&D
2ry α-rat	BV605	405430	Biolegend
IL-10	APC/Cy7	505035	Biolegend
FoxP3	Pacific Blue	126409	Biolegend
CTLA-4	PE/Dazzle 594	106317	Biolegend
IL-9	Alexa 700	IC409N-100ug	R&D
IL-21	PE-Cy7	25-7213-80	ThermoFisher
CD40L	APC	106509	BioLegend

CXCR5	APC-750	145533	BioLegend
PD-1	BV711	135231	BioLegend
IgD	Alexa 647	405707	Biolegend
IL-6	PE	504503	BioLegend
IL-4	BV605	504126	BioLegend
Bcl6	PerCP-Cy5	358507	BioLegend
GATA3	Alexa 488	653807	BioLegend
Tbet	BV785	644835	BioLegend
IFN-g	BV605	505832	BioLegend
Ki-67	Alexa 594	151214	BioLegend
IL-12	V450	561456	BD

Table II-1:List of antibodies used for flow cytometry

References

1. Anderson, C.J., et al., *Hypoxic regulation of telomerase gene expression by transcriptional and post-transcriptional mechanisms.* Oncogene, 2006. **25**(1): p. 61-9.

2. Anderson, P., *Post-transcriptional control of cytokine production.* Nat Immunol, 2008. **9**(4): p. 353-9.

3. Anderson, P., *Post-transcriptional regulons coordinate the initiation and resolution of inflammation.* Nat Rev Immunol, 2010. **10**(1): p. 24-35.

4. Keene, J.D., *RNA regulons: coordination of post-transcriptional events.* Nat Rev Genet, 2007. **8**(7): p. 533-43.

5. Khabar, K.S., *Rapid transit in the immune cells: the role of mRNA turnover regulation.* J Leukoc Biol, 2007. **81**(6): p. 1335-44.

6. Stoecklin, G. and P. Anderson, *Posttranscriptional mechanisms regulating the inflammatory response.* Adv Immunol, 2006. **89**: p. 1-37.

7. Vlasova, M.A. and S.A. Moshkovskii, *Molecular interactions of acute phase serum amyloid A: possible involvement in carcinogenesis.* Biochemistry (Mosc), 2006. **71**(10): p. 1051-9.

8. Anderson, P. and N. Kedersha, *RNA granules: post-transcriptional and epigenetic modulators of gene expression.* Nat Rev Mol Cell Biol, 2009. **10**(6): p. 430-6.

9. Anderson, P., et al., *Post-transcriptional regulation of proinflammatory proteins.* J Leukoc Biol, 2004. **76**(1): p. 42-7.

10. Matoulkova, E., et al., *The role of the 3' untranslated region in post-transcriptional regulation of protein expression in mammalian cells.* RNA Biol, 2012. **9**(5): p. 563-76.

11. Moore, M.J., *From birth to death: the complex lives of eukaryotic mRNAs.* Science, 2005. **309**(5740): p. 1514-8.

12. Guhaniyogi, J. and G. Brewer, *Regulation of mRNA stability in mammalian cells.* Gene, 2001. **265**(1-2): p. 11-23.

13. Ross, J., *mRNA stability in mammalian cells.* Microbiol Rev, 1995. **59**(3): p. 423-50.

14. Mino, T. and O. Takeuchi, *Post-transcriptional regulation of immune responses by RNA binding proteins.* Proc Jpn Acad Ser B Phys Biol Sci, 2018. **94**(6): p. 248-258.

15. Hao, S. and D. Baltimore, *The stability of mRNA influences the temporal order of the induction of genes encoding inflammatory molecules.* Nat Immunol, 2009. **10**(3): p. 281-8.

16. Anderson, P., *Intrinsic mRNA stability helps compose the inflammatory symphony.* Nat Immunol, 2009. **10**(3): p. 233-4.

17. Garcia-Maurino, S.M., et al., *RNA Binding Protein Regulation and Cross-Talk in the Control of AU-rich mRNA Fate.* Front Mol Biosci, 2017. **4**: p. 71.

18. Hentze, M.W., et al., *A brave new world of RNA-binding proteins.* Nat Rev Mol Cell Biol, 2018. **19**(5): p. 327-341.

19. Turner, M. and D.J. Hodson, *An emerging role of RNA-binding proteins as multifunctional regulators of lymphocyte development and function.* Adv Immunol, 2012. **115**: p. 161-85.

20. Nachtergaele, S. and C. He, *The emerging biology of RNA post-transcriptional modifications.* RNA Biol, 2017. **14**(2): p. 156-163.

21. Diaz-Munoz, M.D., et al., *The RNA-binding protein HuR is essential for the B cell antibody response.* Nat Immunol, 2015. **16**(4): p. 415-25.

22. Monzon-Casanova, E., et al., *The RNA-binding protein PTBP1 is necessary for B cell selection in germinal centers.* Nat Immunol, 2018. **19**(3): p. 267-278.

23. Turner, M. and M.D. Diaz-Munoz, *RNA-binding proteins control gene expression and cell fate in the immune system.* Nat Immunol, 2018. **19**(2): p. 120-129.

24. Diaz-Munoz, M.D. and M. Turner, *Uncovering the Role of RNA-Binding Proteins in Gene Expression in the Immune System.* Front Immunol, 2018. **9**: p. 1094.

25. He, X., et al., *Knockdown of polypyrimidine tract-binding protein suppresses ovarian tumor cell growth and invasiveness in vitro.* Oncogene, 2007. **26**(34): p. 4961-8.

26. Wang, C., et al., *Polypyrimidine tract-binding protein (PTB) differentially affects malignancy in a cell line-dependent manner.* J Biol Chem, 2008. **283**(29): p. 20277-87.

27. Wang, H., et al., *c-Myc depletion inhibits proliferation of human tumor cells at various stages of the cell cycle.* Oncogene, 2008. **27**(13): p. 1905-15.

28. Cheung, H.C., et al., *Splicing factors PTBP1 and PTBP2 promote proliferation and migration of glioma cell lines.* Brain, 2009. **132**(Pt 8): p. 2277-88.

29. Sawicka, K., et al., *Polypyrimidine-tract-binding protein: a multifunctional RNA-binding protein.* Biochem Soc Trans, 2008. **36**(Pt 4): p. 641-7.

30. Spriggs, K.A., S.A. Mitchell, and A.E. Willis, *Investigation of interactions of polypyrimidine tract-binding protein with artificial internal ribosome entry segments.* Biochem Soc Trans, 2005. **33**(Pt 6): p. 1483-6.

31. Amir-Ahmady, B., et al., *Exon repression by polypyrimidine tract binding protein.* RNA, 2005. **11**(5): p. 699-716.

32. Xue, Y., et al., *Genome-wide analysis of PTB-RNA interactions reveals a strategy used by the general splicing repressor to modulate exon inclusion or skipping.* Mol Cell, 2009. **36**(6): p. 996-1006.

33. Kafasla, P., et al., *Defining the roles and interactions of PTB.* Biochem Soc Trans, 2012. **40**(4): p. 815-20.

34. Xie, J., et al., *Protein kinase A phosphorylation modulates transport of the polypyrimidine tract-binding protein.* Proc Natl Acad Sci U S A, 2003. **100**(15): p. 8776-81.

35. Romanelli, M.G., E. Diani, and P.M. Lievens, *New insights into functional roles of the polypyrimidine tract-binding protein.* Int J Mol Sci, 2013. **14**(11): p. 22906-32.

36. Vavassori, S. and L.R. Covey, *Post-transcriptional regulation in lymphocytes: the case of CD154.* RNA Biol, 2009. **6**(3): p. 259-65.

37. Matus-Nicodemos, R., et al., *Polypyrimidine tract-binding protein is critical for the turnover and subcellular distribution of CD40 ligand mRNA in CD4+ T cells.* J Immunol, 2011. **186**(4): p. 2164-71.

38. Buckwalter, M.R. and M.L. Albert, *Orchestration of the immune response by dendritic cells.* Curr Biol, 2009. **19**(9): p. R355-61.

39. Dieli, F., *Dendritic cells and the handling of antigen.* Clin Exp Immunol, 2003. **134**(2): p. 178-80.

40. Janeway, C.A., Jr. and K. Bottomly, *Responses of T cells to ligands for the T-cell receptor.* Semin Immunol, 1996. **8**(2): p. 108-115.

41. Elgueta, R., et al., *Molecular mechanism and function of CD40/CD40L engagement in the immune system.* Immunol Rev, 2009. **229**(1): p. 152-72.

42. Xu, J., et al., *Mice deficient for the CD40 ligand.* Immunity, 1994. **1**(5): p. 423-31.

43. Gatto, D. and M.F. Bachmann, *Function of marginal zone B cells in antiviral B-cell responses.* Crit Rev Immunol, 2005. **25**(4): p. 331-42.

44. Stebegg, M., et al., *Regulation of the Germinal Center Response.* Front Immunol, 2018. **9**: p. 2469.

45. Nieuwenhuis, P. and D. Opstelten, *Functional anatomy of germinal centers.* Am J Anat, 1984. **170**(3): p. 421-35.

46. Allen, C.D., T. Okada, and J.G. Cyster, *Germinal-center organization and cellular dynamics.* Immunity, 2007. **27**(2): p. 190-202.

47. MacLennan, I.C., *Germinal centers.* Annu Rev Immunol, 1994. **12**: p. 117-39.

48. Rajewsky, K., *Clonal selection and learning in the antibody system.* Nature, 1996. **381**(6585): p. 751-8.

49. Victora, G.D. and M.C. Nussenzweig, *Germinal centers.* Annu Rev Immunol, 2012. **30**: p. 429-57.

50. Crotty, S., *A brief history of T cell help to B cells.* Nat Rev Immunol, 2015. **15**(3): p. 185-9.

51. Liu, Y.J., et al., *Sites of specific B cell activation in primary and secondary responses to T cell-dependent and T cell-independent antigens.* Eur J Immunol, 1991. **21**(12): p. 2951-62.

52. Manser, T., *Textbook germinal centers?* J Immunol, 2004. **172**(6): p. 3369-75.

53. Pape, K.A., et al., *Visualization of the genesis and fate of isotype-switched B cells during a primary immune response.* J Exp Med, 2003. **197**(12): p. 1677-87.

54. Shinall, S.M., et al., *Identification of murine germinal center B cell subsets defined by the expression of surface isotypes and differentiation antigens.* J Immunol, 2000. **164**(11): p. 5729-38.

55. Wang, Y. and R.H. Carter, *CD19 regulates B cell maturation, proliferation, and positive selection in the FDC zone of murine splenic germinal centers.* Immunity, 2005. **22**(6): p. 749-61.

56. Vuong, B.Q., et al., *A DNA break- and phosphorylation-dependent positive feedback loop promotes immunoglobulin class-switch recombination.* Nat Immunol, 2013. **14**(11): p. 1183-1189.

57. Honjo, T., K. Kinoshita, and M. Muramatsu, *Molecular mechanism of class switch recombination: linkage with somatic hypermutation.* Annu Rev Immunol, 2002. **20**: p. 165-96.

58. Victora, G.D., et al., *Germinal center dynamics revealed by multiphoton microscopy with a photoactivatable fluorescent reporter.* Cell, 2010. **143**(4): p. 592-605.

59. Kurosaki, T., K. Kometani, and W. Ise, *Memory B cells.* Nature Reviews Immunology, 2015. **15**: p. 149.

60. Allen, C.D., et al., *Germinal center dark and light zone organization is mediated by CXCR4 and CXCR5.* Nat Immunol, 2004. **5**(9): p. 943-52.

61. Bannard O, H.R., Allen CD, An J, Nagasawa T, Cyster JG., *Germinal center centroblasts transition to a centrocyte phenotype according to a*

timed program and depend on the dark zone for effective selection. Immunity, 2013. **39**(1097-4180): p. 912-24.

62. Cyster, J.G., et al., *Follicular stromal cells and lymphocyte homing to follicles.* Immunol Rev, 2000. **176**: p. 181-93.

63. Victora, G.D. and L. Mesin.

64. Radmacher, M.D., G. Kelsoe, and T.B. Kepler, *Predicted and inferred waiting times for key mutations in the germinal centre reaction: evidence for stochasticity in selection.* Immunol Cell Biol, 1998. **76**(4): p. 373-81.

65. Koike, T., et al., *The quantity of CD40 signaling determines the differentiation of B cells into functionally distinct memory cell subsets.* Elife, 2019. **8**.

66. Cattoretti, G., et al., *Nuclear and cytoplasmic AID in extrafollicular and germinal center B cells.* Blood, 2006. **107**(10): p. 3967-75.

67. Moldenhauer, G., et al., *AID expression identifies interfollicular large B cells as putative precursors of mature B-cell malignancies.* Blood, 2006. **107**(6): p. 2470-3.

68. Furukawa, K., et al., *Junctional amino acids determine the maturation pathway of an antibody.* Immunity, 1999. **11**(3): p. 329-38.

69. Di Niro, R., et al., *Salmonella Infection Drives Promiscuous B Cell Activation Followed by Extrafollicular Affinity Maturation.* Immunity, 2015. **43**(1): p. 120-31.

70. Stavnezer, J., J.E. Guikema, and C.E. Schrader, *Mechanism and regulation of class switch recombination.* Annu Rev Immunol, 2008. **26**: p. 261-92.

71. Klein, U., et al., *Transcription factor IRF4 controls plasma cell differentiation and class-switch recombination.* Nat Immunol, 2006. **7**(7): p. 773-82.

72. Vinuesa, C.G., I. Sanz, and M.C. Cook, *Dysregulation of germinal centres in autoimmune disease.* Nat Rev Immunol, 2009. **9**(12): p. 845-57.

73. Cerutti, A., *The regulation of IgA class switching.* Nat Rev Immunol, 2008. **8**(6): p. 421-34.

74. Fagarasan, S., et al., *In situ class switching and differentiation to IgA-producing cells in the gut lamina propria.* Nature, 2001. **413**(6856): p. 639-43.

75. Roco, J.A., et al., *Class-Switch Recombination Occurs Infrequently in Germinal Centers.* Immunity, 2019. **51**(2): p. 337-350 e7.

76. Etzioni, A. and H.D. Ochs, *The hyper IgM syndrome--an evolving story.* Pediatr Res, 2004. **56**(4): p. 519-25.

77. Abbott, R.K., et al., *Precursor Frequency and Affinity Determine B Cell Competitive Fitness in Germinal Centers, Tested with Germline-Targeting HIV Vaccine Immunogens.* Immunity, 2018. **48**(1): p. 133-146 e6.

78. Crotty, S., *T Follicular Helper Cell Biology: A Decade of Discovery and Diseases.* Immunity, 2019. **50**(5): p. 1132-1148.

79. Hatzi, K., et al., *BCL6 orchestrates Tfh cell differentiation via multiple distinct mechanisms.* J Exp Med, 2015. **212**(4): p. 539-53.

80. Cunningham, A.F., et al., *Pinpointing IL-4-independent acquisition and IL-4-influenced maintenance of Th2 activity by CD4 T cells.* Eur J Immunol, 2004. **34**(3): p. 686-694.

81. Ozaki, K., et al., *A critical role for IL-21 in regulating immunoglobulin production.* Science, 2002. **298**(5598): p. 1630-4.

82. Reiter, R. and K. Pfeffer, *Impaired germinal centre formation and humoral immune response in the absence of CD28 and interleukin-4.* Immunology, 2002. **106**(2): p. 222-8.

83. Sharpe, A.H. and G.J. Freeman, *The B7-CD28 superfamily.* Nat Rev Immunol, 2002. **2**(2): p. 116-26.

84. Vajdy, M., et al., *Impaired mucosal immune responses in interleukin 4-targeted mice.* J Exp Med, 1995. **181**(1): p. 41-53.

85. Borrow, P., et al., *CD40L-deficient mice show deficits in antiviral immunity and have an impaired memory CD8+ CTL response.* J Exp Med, 1996. **183**(5): p. 2129-42.

86. Renshaw, B.R., et al., *Humoral immune responses in CD40 ligand-deficient mice.* J Exp Med, 1994. **180**(5): p. 1889-900.

87. Whitmire, J.K., et al., *CD40 ligand-deficient mice generate a normal primary cytotoxic T-lymphocyte response but a defective humoral response to a viral infection.* J Virol, 1996. **70**(12): p. 8375-81.

88. Han, S., et al., *Cellular interaction in germinal centers. Roles of CD40 ligand and B7-2 in established germinal centers.* J Immunol, 1995. **155**(2): p. 556-67.

89. Liu, D., et al., *T-B-cell entanglement and ICOSL-driven feed-forward regulation of germinal centre reaction.* Nature, 2015. **517**(7533): p. 214-8.

90. Good-Jacobson, K.L. and M.J. Shlomchik, *Plasticity and heterogeneity in the generation of memory B cells and long-lived plasma cells: the influence of germinal center interactions and dynamics.* J Immunol, 2010. **185**(6): p. 3117-25.

91. Chan, T.D. and R. Brink, *Affinity-based selection and the germinal center response.* Immunol Rev, 2012. **247**(1): p. 11-23.

92. Oracki, S.A., et al., *Plasma cell development and survival.* Immunol Rev, 2010. **237**(1): p. 140-59.

93. Weisel, F.J., et al., *A Temporal Switch in the Germinal Center Determines Differential Output of Memory B and Plasma Cells.* Immunity, 2016. **44**(1): p. 116-130.

94. Toyama, H., et al., *Memory B cells without somatic hypermutation are generated from Bcl6-deficient B cells.* Immunity, 2002. **17**(3): p. 329-39.

95. Obukhanych, T.V. and M.C. Nussenzweig, *T-independent type II immune responses generate memory B cells.* J Exp Med, 2006. **203**(2): p. 305-10.

96. Dogan, I., et al., *Multiple layers of B cell memory with different effector functions.* Nat Immunol, 2009. **10**(12): p. 1292-9.

97. Zuccarino-Catania, G.V., et al., *CD80 and PD-L2 define functionally distinct memory B cell subsets that are independent of antibody isotype.* Nat Immunol, 2014. **15**(7): p. 631-7.

98. Tomayko, M.M., et al., *Cutting edge: Hierarchy of maturity of murine memory B cell subsets.* J Immunol, 2010. **185**(12): p. 7146-50.

99. Kaji, T., et al., *Distinct cellular pathways select germline-encoded and somatically mutated antibodies into immunological memory.* J Exp Med, 2012. **209**(11): p. 2079-97.

100. Takemori, T., et al., *Generation of memory B cells inside and outside germinal centers.* Eur J Immunol, 2014. **44**(5): p. 1258-64.

101. Taylor, J.J., K.A. Pape, and M.K. Jenkins, *A germinal center-independent pathway generates unswitched memory B cells early in the primary response.* J Exp Med, 2012. **209**(3): p. 597-606.

102. Shlomchik, M.J. and F. Weisel, *Germinal center selection and the development of memory B and plasma cells.* Immunol Rev, 2012. **247**(1): p. 52-63.

103. Zotos, D. and D.M. Tarlinton, *Determining germinal centre B cell fate.* Trends Immunol, 2012. **33**(6): p. 281-8.

104. Linterman, M.A., et al., *IL-21 acts directly on B cells to regulate Bcl-6 expression and germinal center responses.* J Exp Med, 2010. **207**(2): p. 353-63.

105. Zotos, D., et al., *IL-21 regulates germinal center B cell differentiation and proliferation through a B cell-intrinsic mechanism.* J Exp Med, 2010. **207**(2): p. 365-78.

106. Good-Jacobson, K.L., et al., *PD-1 regulates germinal center B cell survival and the formation and affinity of long-lived plasma cells.* Nat Immunol, 2010. **11**(6): p. 535-42.

107. Han, W., et al., *Novel Molecular Mechanism of Regulation of CD40 Ligand by the Transcription Factor GLI2.* J Immunol, 2017. **198**(11): p. 4481-4489.

108. Lindgren, H., K. Axcrona, and T. Leanderson, *Regulation of transcriptional activity of the murine CD40 ligand promoter in response to signals through TCR and the costimulatory molecules CD28 and CD2.* J Immunol, 2001. **166**(7): p. 4578-85.

109. La Porta, J., et al., *The RNA-Binding Protein, Polypyrimidine Tract-Binding Protein 1 (PTBP1) Is a Key Regulator of CD4 T Cell Activation.* PLoS One, 2016. **11**(8): p. e0158708.

110. Vavassori, S., et al., *In vivo post-transcriptional regulation of CD154 in mouse CD4+ T cells.* Eur J Immunol, 2009. **39**(8): p. 2224-32.

111. Lesley, R., et al., *Naive CD4 T cells constitutively express CD40L and augment autoreactive B cell survival.* Proc Natl Acad Sci U S A, 2006. **103**(28): p. 10717-22.

112. Cibrian, D. and F. Sanchez-Madrid, *CD69: from activation marker to metabolic gatekeeper.* Eur J Immunol, 2017. **47**(6): p. 946-953.

113. Ziegler, S.F., F. Ramsdell, and M.R. Alderson, *The activation antigen CD69.* Stem Cells, 1994. **12**(5): p. 456-65.

114. Whitmire, J.K., et al., *CD40-CD40 ligand costimulation is required for generating antiviral CD4 T cell responses but is dispensable for CD8 T cell responses.* J Immunol, 1999. **163**(6): p. 3194-201.

115. Mesin, L., J. Ersching, and G.D. Victora, *Germinal Center B Cell Dynamics.* Immunity, 2016. **45**(3): p. 471-482.

116. Finney, J., et al., *Germinal center responses to complex antigens.* Immunol Rev, 2018. **284**(1): p. 42-50.

117. Harwood, N.E. and F.D. Batista, *The antigen expressway: follicular conduits carry antigen to B cells.* Immunity, 2009. **30**(2): p. 177-9.

118. Batista, F.D. and N.E. Harwood, *The who, how and where of antigen presentation to B cells.* Nat Rev Immunol, 2009. **9**(1): p. 15-27.

119. Okada, T., et al., *Antigen-engaged B cells undergo chemotaxis toward the T zone and form motile conjugates with helper T cells.* PLoS Biol, 2005. **3**(6): p. e150.

120. Chan, T.D., et al., *Antigen affinity controls rapid T-dependent antibody production by driving the expansion rather than the differentiation or extrafollicular migration of early plasmablasts.* J Immunol, 2009. **183**(5): p. 3139-49.

121. Coffey, F., B. Alabyev, and T. Manser, *Initial clonal expansion of germinal center B cells takes place at the perimeter of follicles.* Immunity, 2009. **30**(4): p. 599-609.

122. MacLennan, I.C., et al., *Extrafollicular antibody responses.* Immunol Rev, 2003. **194**: p. 8-18.

123. Victora, G.D. and L. Mesin, *Clonal and cellular dynamics in germinal centers.* Curr Opin Immunol, 2014. **28**: p. 90-6.

124. Hirth, G., et al., *Regulation of the Germinal Center Reaction and Somatic Hypermutation Dynamics by Homologous Recombination.* J Immunol, 2019. **203**(6): p. 1493-1501.

125. Neuberger, M.S. and C. Milstein, *Somatic hypermutation.* Curr Opin Immunol, 1995. **7**(2): p. 248-54.

126. Hastey, C.J., et al., *Delays and diversions mark the development of B cell responses to Borrelia burgdorferi infection.* J Immunol, 2012. **188**(11): p. 5612-22.

127. Cunningham, A.F., et al., *Salmonella induces a switched antibody response without germinal centers that impedes the extracellular spread of infection.* J Immunol, 2007. **178**(10): p. 6200-7.

128. Stewart, I., et al., *Germinal Center B Cells Replace Their Antigen Receptors in Dark Zones and Fail Light Zone Entry when Immunoglobulin Gene Mutations are Damaging.* Immunity, 2018. **49**(3): p. 477-489 e7.

129. Fagarasan, S. and T. Honjo, *T-Independent immune response: new aspects of B cell biology.* Science, 2000. **290**(5489): p. 89-92.

130. Fagarasan, S., et al., *Adaptive immune regulation in the gut: T cell-dependent and T cell-independent IgA synthesis.* Annu Rev Immunol, 2010. **28**: p. 243-73.

131. Sia, J.K., et al., *Engaging the CD40-CD40L pathway augments T-helper cell responses and improves control of Mycobacterium tuberculosis infection.* PLoS Pathog, 2017. **13**(8): p. e1006530.

132. Cumano, A. and K. Rajewsky, *Clonal recruitment and somatic mutation in the generation of immunological memory to the hapten NP.* Embo j, 1986. **5**(10): p. 2459-68.

133. Blier, P.R. and A. Bothwell, *A limited number of B cell lineages generates the heterogeneity of a secondary immune response.* J Immunol, 1987. **139**(12): p. 3996-4006.

134. Allen, D., et al., *Antibody engineering for the analysis of affinity maturation of an anti-hapten response.* Embo j, 1988. **7**(7): p. 1995-2001.

135. Lopez-Saucedo, C., et al., *CD40 Ligand Deficient C57BL/6 Mouse Is a Potential Surrogate Model of Human X-Linked Hyper IgM (X-HIGM) Syndrome for Characterizing Immune Responses against Pathogens.* Biomed Res Int, 2015. **2015**: p. 679850.

136. Durandy, A., S. Kracker, and A. Fischer, *Primary antibody deficiencies.* Nat Rev Immunol, 2013. **13**(7): p. 519-33.

137. van Zelm, M.C., et al., *Human CD19 and CD40L deficiencies impair antibody selection and differentially affect somatic hypermutation.* J Allergy Clin Immunol, 2014. **134**(1): p. 135-44.

138. Lanzavecchia, A., *Antigen-specific interaction between T and B cells.* Nature, 1985. **314**(6011): p. 537-9.

139. Shinnakasu, R. and T. Kurosaki, *Regulation of memory B and plasma cell differentiation.* Curr Opin Immunol, 2017. **45**: p. 126-131.

140. Suan, D., et al., *CCR6 Defines Memory B Cell Precursors in Mouse and Human Germinal Centers, Revealing Light-Zone Location and Predominant Low Antigen Affinity.* Immunity, 2017. **47**(6): p. 1142-1153 e4.

141. Maddaly, R., et al., *Receptors and signaling mechanisms for B-lymphocyte activation, proliferation and differentiation--insights from both in vivo and in vitro approaches.* FEBS Lett, 2010. **584**(24): p. 4883-94.

142. Ersching, J., et al., *Germinal Center Selection and Affinity Maturation Require Dynamic Regulation of mTORC1 Kinase.* Immunity, 2017. **46**(6): p. 1045-1058 e6.

143. Castan, J., et al., *Accumulation of CTLA-4 expressing T lymphocytes in the germinal centres of human lymphoid tissues.* Immunology, 1997. **90**(2): p. 265-71.

144. Shulman, Z., et al., *Dynamic signaling by T follicular helper cells during germinal center B cell selection.* Science, 2014. **345**(6200): p. 1058-62.

145. Johnston, R.J., et al., *Bcl6 and Blimp-1 are reciprocal and antagonistic regulators of T follicular helper cell differentiation.* Science, 2009. **325**(5943): p. 1006-10.

146. Carvalho, L.J., et al., *Germinal center architecture disturbance during Plasmodium berghei ANKA infection in CBA mice.* Malar J, 2007. **6**: p. 59.

147. Inoue, T., et al., *The transcription factor Foxo1 controls germinal center B cell proliferation in response to T cell help.* J Exp Med, 2017. **214**(4): p. 1181-1198.

148. Ise, W., et al., *T Follicular Helper Cell-Germinal Center B Cell Interaction Strength Regulates Entry into Plasma Cell or Recycling Germinal Center Cell Fate.* Immunity, 2018. **48**(4): p. 702-715 e4.

149. Weinstein, J.S., et al., *TFH cells progressively differentiate to regulate the germinal center response.* Nat Immunol, 2016. **17**(10): p. 1197-1205.

150. Sidiropoulos, P.I. and D.T. Boumpas, *Lessons learned from anti-CD40L treatment in systemic lupus erythematosus patients.* Lupus, 2004. **13**(5): p. 391-7.

151. Karnell, J.L., et al., *Targeting the CD40-CD40L pathway in autoimmune diseases: Humoral immunity and beyond.* Adv Drug Deliv Rev, 2019. **141**: p. 92-103.